

December 2014

Spatial Dimensions of Tower Karst and Cockpit Karst: A Case Study of Guilin, China

Wei Huang

University of Wisconsin-Milwaukee

Follow this and additional works at: <https://dc.uwm.edu/etd>

 Part of the [Geographic Information Sciences Commons](#), and the [Geomorphology Commons](#)

Recommended Citation

Huang, Wei, "Spatial Dimensions of Tower Karst and Cockpit Karst: A Case Study of Guilin, China" (2014). *Theses and Dissertations*. 626.

<https://dc.uwm.edu/etd/626>

This Dissertation is brought to you for free and open access by UWM Digital Commons. It has been accepted for inclusion in Theses and Dissertations by an authorized administrator of UWM Digital Commons. For more information, please contact open-access@uwm.edu.

**SPATIAL DIMENSIONS OF TOWER KARST AND COCKPIT KARST:
A CASE STUDY OF GUILIN, CHINA**

by

Wei Huang

A Dissertation Submitted in
Partial Fulfillment of the
Requirements for the Degree of

Doctor of Philosophy
in Geography

at

The University of Wisconsin-Milwaukee

December 2014

ABSTRACT

SPATIAL DIMENSIONS OF TOWER KARST AND COCKPIT KARST: A CASE STUDY OF GUILIN, CHINA

by

Wei Huang

The University of Wisconsin-Milwaukee, 2014

Under the Supervision of Professor Michael J. Day

Abstract

Tower karst (fenglin) and cockpit karst (fengcong) are two globally important representative styles of tropical karst. Previously proposed sequential and parallel development models are preliminary, and geomorphological studies to date do not provide enough satisfactory evidence to delineate the spatial and temporal relation between the two landscapes. This unclear interpretation of tower-cockpit relationships not only obscures understanding of the process-form dynamics of these tropical karst landforms, but also confuses their definition. Moreover, previous technological limitations, as well as the fragmental nature of the karst landscapes, has limited incorporation of geologic and other data into broad geospatial frameworks based on geographic information science (GIS) and remote sensing (RS), with such data being spatially and temporally disparate. This study incorporates various data sources to

address the fenglin-fengcong relationship, particularly the recently postulated “edge effect”, which has not been examined in detail previously and which may hinge upon the interaction of multiple environmental variables, including geomorphology, vegetation and hydrology. To address these issues, this research combines geographic, geologic and hydrologic data, using GIS and RS technologies to test quantitatively the “edge effect” hypothesis.

Specifically, there are four inter-related objectives of this study. The first is to develop a method to effectively differentiate fenglin and fengcong. The second is to extract optimally the vegetation information from satellite imagery, and investigate the correlation between tropical karst topography and its vegetation. The third is to combine the regional hydrologic data and solute transport models to estimate geochemicals control of fenglin and fengcong. The fourth one, perhaps the most important, is to test the “edge effect” hypothesis using the results from the other three objectives.

There are several significant conclusions. First, DEM data are very useful for extracting profiles of complex surface landforms from satellite imagery. Second, the vegetation distribution varies between tower karst and cockpit karst and the differences correlate with topographic characteristics. The under-representation of vegetation on the south-southwest aspect of tower karst is remarkable, and its overall distribution is both less abundant and dispersed than in cockpit karst. Third, the “edge effect” exists in the Guilin area, with variable intensity and extension in different dimensions.

In summary, the major contributions of the study include the following. First, the study has developed a method to classify fenglin-fengcong tropical karst effectively, even with the presence of shadows that would otherwise hinder traditional classification. Second,

the study showed a variance of vegetation vitality within aspects of fenglin that might relate to its geomorphic difference from fengcong. Third, the study combined groundwater and solute transport models to estimate bicarbonate distributions, representing a novel systematic and quantitative approach to tropical karst studies.

© Copyright by Wei Huang, 2014

All Rights Reserved

Dedicated to my parents...

TABLE OF CONTENTS

ABSTRACT	ii
TABLE OF CONTENTS	vii
LIST OF FIGURES	ix
LIST OF TABLES	xi
ACKNOWLEDGMENTS	xii
CHAPTER 1 INTRODUCTION	1
CHAPTER 2 DIFFERENTIATING TOWER KARST (FENGLIN) AND COCKPIT KARST (FENGCONG) USING DEM CONTOUR, SLOPE AND CENTROID	7
2.1 Introduction	7
2.2 Study area and data	14
2.3 Methodology	18
2.4 Results and Discussion	22
2.5 Conclusion	28
CHAPTER 3 INVESTIGATION OF VEGETATION ON SURFACE KARST USING TOPOGRAPHIC CORRECTION, SHADOW RETRIEVAL AND VEGETATION INDEX	29
3.1 Introduction	29
3.2 Study area and data	33
3.3 Methodology	34
3.4 Results and Discussion	38
3.5 Conclusion	44
CHAPTER 4 HYDROLOGIC CONTROLS ON DEVELOPING TOWER KARST AND COCKPIT KARST	45
4.1 Introduction	45
4.2 Study area and data	49
4.3 Methodology	52
4.4 Results and Discussion	58
4.5 Conclusion	62
CHAPTER 5 EDGE EFFECT	62
5.1 Introduction	62

5.2 Study area and data	65
5.3 Methodology	65
5.4 Results and discussions	66
5.5 Conclusion	75
CHAPTER 6 CONCLUSIONS	76
6.1 Summary	76
6.2 Contribution	77
6.3 Future research	78
REFERENCES	79
CURRICULUM VITAE	98

LIST OF FIGURES

Figure 1. Karst area of China.....	3
Figure 2. Four-phase genetic pattern of the erosion of karst surface (after Jakucs 1977) ..	9
Figure 3. Location of the study area	14
Figure 4. Distribution of fenglin/fengcong on the elevation map (Elevation unit: m)	17
Figure 5. Flow chart of the methodology.....	20
Figure 6. Example of karst landform classification	23
Figure 7. Verification of the classification result using Google Earth (Landscapes surrounded by blue circles are tower karsts; landscapes surrounded by red circles are cockpit karsts)	24
Figure 8. Box charts of six different morphological indices (TK: tower karst, CK: Cockpit karst).....	27
Figure 9. Location of the study area	34
Figure 10. Methodology Flow chart	35
Figure 11. (a) Landsat Imagery without topographic correction. (b) Landsat imagery with topographic correction (Band combination: RGB 642).....	39
Figure 12. (a) Black shadows on the Landsat Imagery. (b) Shadows detected on the Landsat imagery with purple highlighted (Band combination: RGB 642).....	40
Figure 13. Scatterplots of NDVI and karst topography in tower karst and cockpit karst.	42
Figure 14. Windrose diagram of NDVI-Aspect on tower karst and cockpit karst	42
Figure 15. The absence of vegetation at the south aspect of tower karst (Photo Image was taken at the field survey of Guilin on Aug 2011)	44
Figure 16. Study area on the elevation map.....	50
Figure 17. Annual precipitation of the study area.....	51
Figure 18. Annual temperature of the study area.....	51
Figure 19. Annual runoff of the study area.....	51
Figure 20. Methodology of delineating of watershed.....	53
Figure 21. Hydrological chart of fengcong depression system (After Guilin karst geology, 1988)	54
Figure 22. Hydrological chart of fenglin plain system (After Guilin karst geology, 1988)	54
Figure 23. Comparison of Annual Runoff and Annual Runoff.....	55
Figure 24. Bicarbonate estimation from solute transport model.....	58

Figure 25. Soil types in the study area.....	59
Figure 26. Distribution of pressure (h) in different depth of sample sites.....	60
Figure 27.Solute transport of bicarbonate.....	61
Figure 28. Bicarbonate Concentration in the study area.....	61
Figure 29.Global Moran's I for Fenglin in vertical direction.....	72
Figure 30. Global Moran's I for Fenglin in horizontal direction	73
Figure 31. Global Moran's I for Fengcong in vertical direction	74
Figure 32. Global Moran's I for Fengcong in horizontal direction.....	74

LIST OF TABLES

Table 1. Confusion matrix of tower and cockpit karst classification	25
Table 2. Descriptive statistics of towers and cockpits	26
Table 3. Digital value (DN) statistics of samples from shadow areas and non-shadow areas	41
Table 4. Correlation between tower karst latitude and other variables.....	67
Table 5. Model summary between tower karst latitude and other variables	67
Table 6. Model coefficients between tower karst latitude and other variables.....	67
Table 7. Correlation between tower karst longitude and other variables	68
Table 8. Model summary between Tower karst longitude and other variables	68
Table 9. Model coefficients between tower karst longitude and other variables.....	69
Table 10. Correlation between cockpit karst latitude and other variables	69
Table 11. Model summary between cockpit karst latitude and other variables.....	70
Table 12. Model coefficient between cockpit karst latitude and other variables.....	71
Table 13. Correlation between cockpit karst longitude and other variables.....	71
Table 14. Model summary between cockpit karst longitude and other variables.....	71
Table 15. Model coefficients between cockpit karst longitude and other variables.....	72

ACKNOWLEDGMENTS

I would like to express my deepest gratitude to my advisor, Professor Mick Day. The accomplishment of the dissertation would have been impossible without his sincere help and patient direction. Suggestions and guidance from him will become a lifetime treasure in my future life. Special thanks also to my advisory committee members, UWM Professors Changshan Wu, Glen Fredlund and Zengwang Xu, and Professor Daoxian Yuan, of the Institute of Karst Geology, for their valuable suggestions and constructive comments on my dissertation work.

I also appreciate all the people who helped me during my graduate study: Professor Mark Schwartz, Dr. Patti Day, Professors Arthur and Margaret Palmer of the State University of New York – Oneonta, Professor Ryan Holifield, Professor Kristin Sziarto, Dr. Jonathan Hanes, Professor Anne Bonds, Professor Hyejin Yoon, Professor Woonsup Choi, Dr. Alison Donnelly, the Director of UWM's Cartography and GIS Center Donna Genzmer, Professor Judith Kenny, and Program Associate Niko Papakis. In addition, I also extend my thanks to former and current colleagues at UWM, Chengbin Deng, Rong Yu, Wenliang Li, Yingbin Deng, Miao Li, Alarico Fernandes, Nick Padilla, Andrea Kuhlman, Ashley Murray, I-Hui, Lin, Yang Song, and Wei Xu, for their support and help. Last but not the least, my parents deserve my very special thanks for their consistent encouragement and their support in my life.

CHAPTER 1 INTRODUCTION

Tower karst (fenglin) and cockpit karst (fengcong) are two fundamental representative landscape styles in tropical karst. Previous studies have proposed both sequential and parallel models to explain the evolution of these two karst landscapes, but neither group of models provides a totally convincing explanation of the genesis and evolution of existing tower and cockpit karst regions. This unclear interpretation of tower-cockpit relationships not only obscures the understanding of the process-form dynamics in such karst landscapes, but also confuses the definition of the two types. In addition, prior technological limitations, as well as the fragmented nature of karst landscape, have precluded the incorporation of much relevant geologic and other data into broad geospatial frameworks using GIS and RS techniques, with much of the data scattered and poorly integrated both spatially and temporally. To address these issues, this research combines geographic, geologic and hydrologic data with the most recent GIS and remote sensing technologies to generate integrated, novel and useful quantitative geomorphological measures.

Specifically, there are three purposes of the research. The first is to use contemporary GIS and RS techniques to combine hydrologic, geologic and lithologic data from previous studies to examine the karst landscape of Guilin, China, which is arguably the World's best example of tower-cockpit karst. The second aim is to develop an effective method to differentiate fengling and fengcong landforms. The third goal is to test a hypothesis about the existence of an "edge effect" relating to fenglin and fengcong,

which will help to illustrate the tower-cockpit relationship, not only in the area of Guilin, but also elsewhere.

The term “karst” is derived from the German name for the “kras” region of Slovenia, where landscapes dominated by carbonate rock dissolution were first identified (refs). The term has been used both to describe the processes of chemical dissolution of soluble rocks and associated mechanical processes, such as subsidence and collapse, and to delineate the landforms and landscapes resulting from these processes (Yuan 1998). Thus, the term “karst” broadly includes karst processes, karst features and karst regions.

There is an apparent disparity of karst landscape distribution around the world. The largest areas are in North America, in the Alpine fold region of Europe and in Southeast Asia, particularly in China, Thailand and Vietnam. There are also important karst areas in western Asia and North Africa. While karst occurs in southern Africa, South America, Australia, New Zealand and the Pacific, it is far more extensive in the northern hemisphere than in its southern counterpart, reflecting the worldwide distribution of carbonate rocks (Sweeting, 1972).

Soluble carbonate rocks cover over 3.4 million square kilometers in China, which is approximately one third of the total territory (Figure 1). Among this vast karst landscape, the humid tropical and subtropical area of southern China possesses the most extensive outcrop of limestones and dolostones, and exhibits the most dramatic karst landscape. Differing from the “classical” karst areas of Europe and the more subdued karst of North America, the karst topography of mainland China is unique from a global perspective. It is promoted by a combination of favorable geomorphic elements: old, hard, compact carbonate rocks, strong uplift in the Cenozoic Era, no continental ice sheet scouring

during the Pleistocene, and the abundance of water and heat in the East Asia Monsoon region (Yuan, 1991). Visiting Guilin in the 1970s, Sweeting (1978) enumerated three conditions that favored the development of karst in China: (1) large areas and great thickness of pure limestones uninterrupted by any significant intercalation of other rocks; (2) a warm and wet climate over a long period, uninterrupted by intense cold phases (glaciation); (3) neo-tectonic uplift in the later phases of the Tertiary and Quaternary periods. Configured by the Qinghai-Tibet plateau and the Qinling-Dabieshan Range, three main karst areas can be identified on the basis of topographic and climatic setting: the humid subtropical karst in South China, the arid and semiarid karst in North China and the high mountain karst in Southwest China (Yuan, 1998).

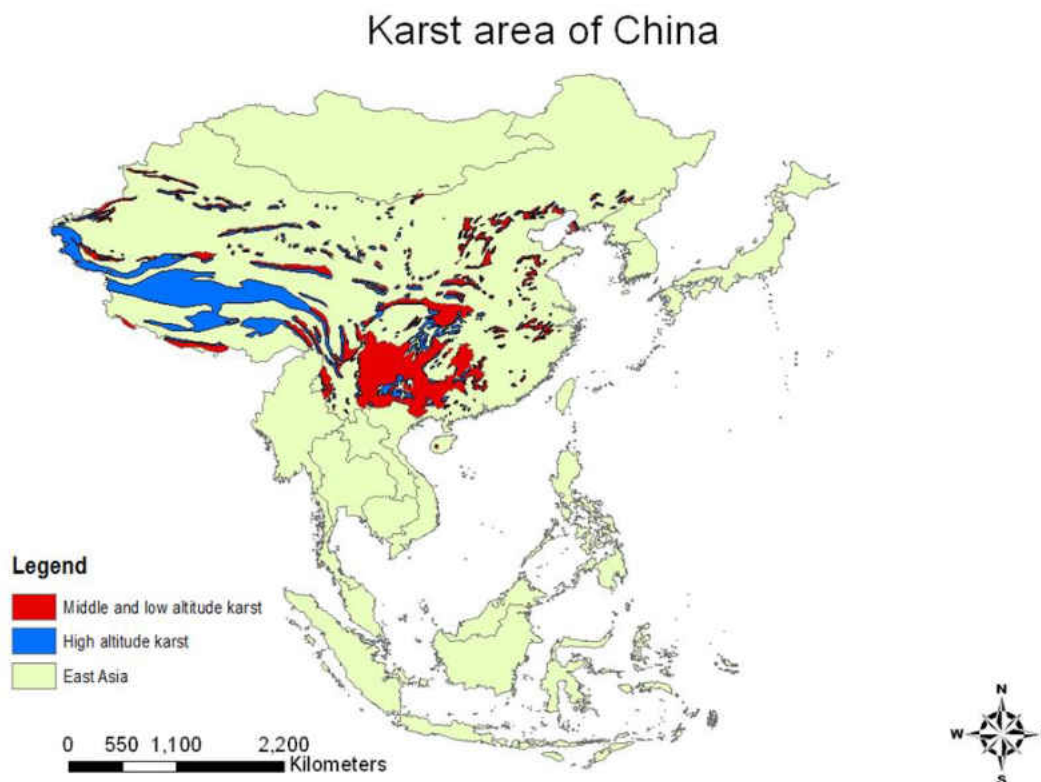


Figure 1. Karst area of China

Data source: School of Environment, the University of Auckland

In south China, the physical strength and coherence of the carbonate rocks have a significant influence on karst formation and landform development. In particular, at the surface, they give rise to accentuated cockpit karst (fengcong) massifs and to spectacular karst towers (fenglin) protruding from alluvial plains. Beneath the surface, they provide the necessary support for large subterranean features such as underground streams and cave chambers (Yuan, 1998). Elsewhere in the World, there is tower karst in Southeast Asia, Central America and the Caribbean, but the towers there are generally lower and rounded, being formed in Tertiary porous carbonate rocks (Troester, 1992).

Guilin is World-famous for its prominent tower karst (fenglin) landscape, which in terms of tower size, diversity, concentration and extent is unequalled both in China and the World. It is regarded as the most beautiful and iconic scenery in China (Sweeting, 1995). The karst array, especially the tower karst near the Li River, where steep cliffs tower over the river, has created dramatic scenery that has been an inspiration to Chinese painters for centuries. The scenery of the Guilin karst, with needle and tower-like hills of limestone towering above the plains has greatly influenced the development of Chinese art and made it World-famous (Swann, 1956).

There are several problems in the study of tower karst in Guilin and elsewhere in the World. The first problem comes from the understanding of tower karst and cockpit karst. Chinese geomorphologists distinguish two groups of tropical karst landscapes: 'fenglin' or 'peak forest' and 'fengcong' or 'peak cluster' (Zhang 1981, Yuan 1981). The former are individual isolated residual hills rising from flood or corrosion plains and which are related to tower karst in western terms. There is a generally accepted interchangeability

between the Chinese word fenglin and the western term tower karst, even though they are defined by different parameters. Almost all true tower karst can be described as fenglin, though the latter term does include some landscapes that contain conical hills instead of steep sided towers (Zhu, 2005). Such interchangeability works extremely well in the case of the residual hills, or towers, which in fenglin are simply erosional remnants in a planar area usually dominated by allogenic fluvial drainage and an alluviated surface (Day and Tang, 2004). On the other hand, fengcong refers to groups of residual hills sharing a common bedrock basement and incorporating closed depressions between the clusters of peaks – landscape to which several western terms have been applied. Waltham (2008) insisted that the word fengcong is equivalent to the western term cone karst based on the morphologies of the residual hills. Day and Huang (2009) proposed that cockpit karst is a more appropriate equivalent than cone karst because of its emphasis on the active geomorphological areas between the residual hills. Therefore, it is necessary to distinguish fenglin and fengcong not only on the grounds of morphological differences but also from the perspective of the terminology applied to the areas within which they are located.

A second problem relates to the evolutionary paths of tower karst and cockpit karst, and especially the relationship between them. This has been a long-term debate over two sets of hypotheses and models that have proved controversial among karst geomorphologists. Broadly, sequential models have been based upon Davis's theory of a Geographical Cycle (1899), and have treated tower karst and cockpit karst as different stages of landscape evolution (Sweeting, 1958, 1990; Gerstenhauer, 1960; Song et al., 1983; Williams, 1985; He, 1986). These models suggest that tower karst has evolved from

cockpit karst, and that thus the former is an “older” stage of the latter. By contrast, parallel models have proposed that both tower karst and cockpit karst have evolved simultaneously without distinctive erosional stages (Verstappen, 1960, Balazs, 1968; Yuan 1981, 1986; Williams, 1986; Yuan et al., 1990; Tan 1992; Sweeting, 1995 and Zhu et al., 1988). Both groups of hypotheses have been mostly based on qualitative field observation rather than detailed quantitative evidence from field measurements, and neither of them appear to fully explain the origin and development of the tower karst in the Guilin area. Perhaps surprisingly, the fengcong karst in Guilin actually occupies a larger distribution area than does the fenglin karst (Zhu, 2005). In part, this has led to the suggestion that there is an “edge effect” (Day and Huang, 2009), with fenglin developing around the periphery of fengcong, and this suggestion offers a fresh perspective from which to investigate whether fenglin has evolved from fengcong or whether they have parallel evolutionary paths.

The third problem relates to spatial scales, technological changes and data integration. Previous studies of cockpit and tower karst topography have focused on individual and assembled morphology and classification, and have used these, largely qualitative descriptions of small-scale areas as the basis for landscape evolution interpretation. In the context of Guilin, Sweeting (1978) noted that the sequential model, which dominated the thought of Chinese geographers, led them to divide the landscape of Guilin into three different stages: fengcong, fenglin and dufeng (isolated peaks), without any quantitative basis. In addition, due to technological limitations and the fragmental nature of the karst landscape, geomorphologists did not adequately combine material (geological) and

geomorphological process data into a broad geospatial frame, with previous studies being disparate in focus and scope.

With the rapid recent development of RS and GIS technologies, it is important to apply such technologies to determine how they can advance geomorphological research on tower and cockpit karst. Detailed GIS datasets and increasing spectral resolution of remotely sensed imageries should provide a deeper insight into, for example, identifying individual tower and cockpit features in the Guilin karst and non-karst landscapes, and incorporating such spatial data with recent hydrological evaluations. This will allow for testing of such hypotheses as that concerning the “edge effect”.

CHAPTER 2 DIFFERENTIATING TOWER KARST (FENGLIN) AND COCKPIT KARST (FENGCONG) USING DEM CONTOUR, SLOPE AND CENTROID

2.1 Introduction

Tower karst (fenglin) consists of isolated limestone towers/hills, often with vertical flanks rising from alluvial plains (Zeng 1982; Day and Tang 2004). Cockpit karst (fengcong), on the other hand, involves similar dimension enclosed depressions surrounded by overlapping hills and ridges. (Day 2004a; Day and Chenoweth 2004; Yuan 1984; Zhu et al. 2013). These two landforms are the two most spectacular and diagnostic landscape styles in tropical karst environments, where high temperatures and abundant precipitation provide a favorable environment for rapid and prolonged corrosion. Typical examples can also be found in Southeast Asia, Central America and the Caribbean, although the

towers there are lower and rounded, being formed in weaker, porous Tertiary carbonate rocks (Troester 1992).

Studying the relationships between fenglin and fengcong holds the key to understanding tropical karst evolution (Sweeting 1972; Smart et al. 1986; Zhu 1988; Yuan 1991 and 2004; Ford and Williams 2007; Waltham 2008). Jakucs (1977) proposed a four-phase genetic model (Figure 2) to describe the erosion of a karst surface: (1) soil and regolith are removed and accumulate in karst depressions, (2) tectonic uplift occurs as the karst plain becomes corroded with cockpit karst, (3) as the uplift ceases or decelerates, floodplains widen and isolate cockpit karst, (4) when residual blocks widen at the level of water table, they are eventually isolated as towers or tower groups. Yuan (1985) reviewed explanations proposed for the evolution of tower karst, among which are two extreme possibilities: (1) tower karst evolves directly and independently of any previous morphology, given favorable lithological, relief and climatic circumstances, (2) the geometry of tower karst depends explicitly on the topographic characteristics inherited directly from a previous phase, such as cockpit karst relief, but becomes increasingly independent of this inheritance as erosion proceeds.

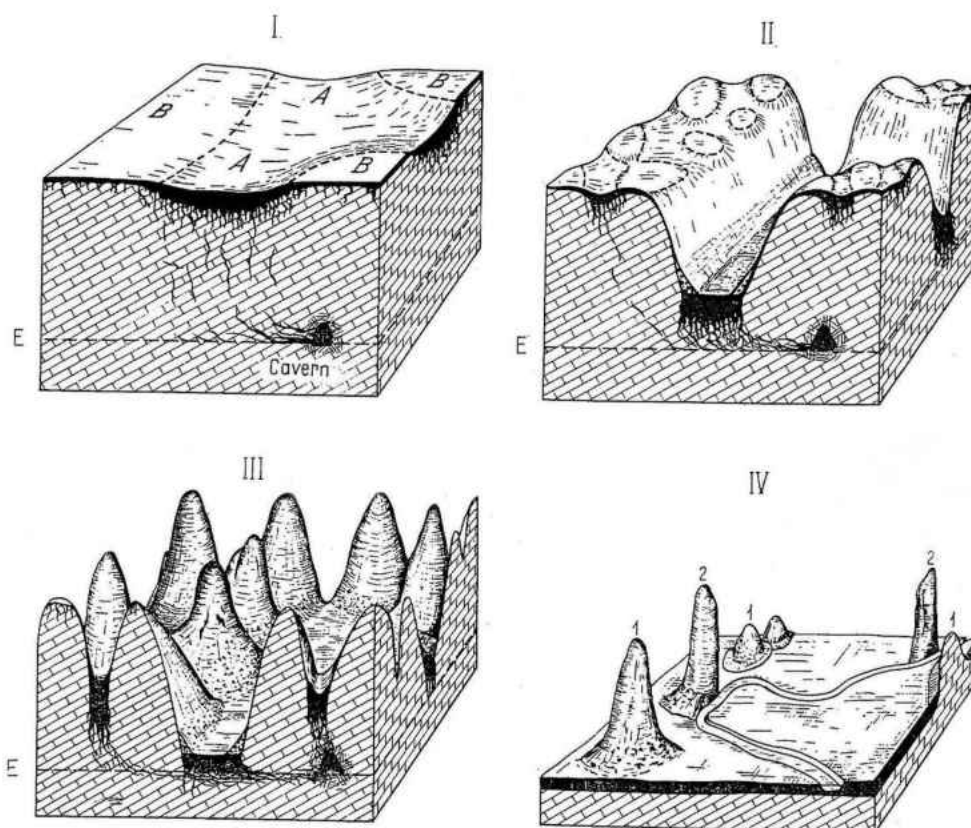


Fig. 45. Four-phase genetic pattern of the erosion of karst surfaces in the tropics

Phase I: Soil and related waste is removed from the hummocks and deposited in the depressions of a pre-karst surface, resulting in more intense karstification in the areas marked A as compared to the areas marked B (E represents the baselevel of erosion)

Phase II: Intense karst corrosion under the soil cover in the A-areas causes the karst surface to be lowered increasingly faster than under the B-areas: the B-areas become progressively dissimilar to the A-areas too, owing to cumulative effects (e.g. to sub-areal erosion, the focal point of our considerations)

Phase III: Phase of evolution of the tropical cone karst. The B-areas themselves are so reduced in size that they are divided into peaks and ridges where the rate of vertical erosion is low, as any soil formed is soon swept off the steep hill-sides. The karst cone thus evolves as a permanent form of the tropical karst, whose base, placed where soil may accumulate, can erode ten times faster than at its summit

Phase IV: Lateral erosion and corrosion of the rivers forming in the A-areas at the baselevel of erosion develop the karst cones into karst towers by undercutting. In the process, the formerly underground streams develop surface beds in the A-areas and these latter are widened into intermontane plains, while the ground plans of the karst inselbergs left over from the former B-areas are gradually reduced (1 — cone karst; 2 — tower karst)

Figure 2. Four-phase genetic pattern of the erosion of karst surface (after Jakucs 1977)

There has been much debate as to whether the two styles follow sequential or simultaneous development paths (Williams 1987; Zhu 1988; Yuan 2004; Waltham 2008), although the consensus now appears to be that the two forms can and do develop contemporaneously, with fenglin, which in many locations occurs on the periphery of fengcong, involving greater fluvial influence (McDonald 2002; Tang and Day 2000; Day 2002; Day and Huang 2009).

The distinction between the two styles is not clear-cut, however, and their morphological similarities and spatial coexistence make it difficult in some locations to differentiate between them, particularly where local conditions result in intermediate forms that fit neatly into neither category. For example, some residual hills or towers in fenglin share common bases, and flat-floored depressions may isolate individual fengcong hills. Terminology apart, both tower and cockpit karst contain assemblages of residual hills of variable morphology, some of which are connected by ridges, others of which are isolated by equally variable depressions (Day 1978, 1981 and 2004a).

Initial approaches to differentiating between cockpit karst and tower karst focused on the morphology and spatial arrangement of the residual hills, which are a common denominator of both styles. Balazs (1973) assigned the hills to four “type area” categories on the basis of their $R_{d/h}$ or diameter/height ratio: Yangshuo ($D/H < 1.5$), Organos ($D/H 1.5-3.0$), Sewu ($D/H 3-8$) and Tual ($D/H > 8$), suggesting that the relatively high and steep hills were more typical of fenglin, although they might be in a minority even here, a suggestion confirmed in a tower karst area of Puerto Rico, where the Yangshuo type accounted for only 2% of the hills measured (Day 1978). While residual hill

morphologies may provide some insights into the development of tower and cockpit karst, clearly they provide no distinction between the two styles, except possibly when combined with the spatial arrangement of the hills and the intervening depressions, for example to derive a generic three-fold classification of tropical karst landscape styles: Type I, in which enclosed depressions dominate and are interspersed with subdued hills; type II, in which enclosed depressions and residual hills attain approximately equal prominence; and type III, in which isolated residual hills dominate intervening near-planar surfaces (Day 1978 and 1981). Following this approach, fengcong/cockpit karst belongs to type II, whereas tower karst belongs to type III.

Another approach attempted to differentiate tower and cockpit karst on the basis of hill summit elevations (Gellert 1962), but statistical analysis of over 600 summits in the Guilin area demonstrated that there was no distinct correlation between summit elevations and styles (Zhu et al. 1980). Furthermore, it is clear that the terms tower karst and cockpit karst actually refer to spectra of landscapes, with there being, for example, four major types of tower karst: (1) residual hills protruding from a planed carbonate surface veneered by alluvium; (2) residual hills emerging from carbonate inliers in a planned surface cut mainly across non-carbonate rocks; (3) carbonate hills protruding through an aggraded surface of clastic sediments that buries the underlying karst topography; (4) isolated carbonate towers rising from steeply sloping pedestal bases of various lithologies (Ford and Williams, 2007).

Although residual hills (and ridges) are integral to both cockpit and tower karst landscapes, the dynamic foci of geomorphic processes are the areas between them: sinkholes of variable morphology, erosional valleys, flat-floored depressions or alluviated

plains. Their role is critical in karst style differentiation, and ultimately it is the relationships between the residuals and the intervening depressions that distinguish between cockpit karst and tower karst. Broad morphometric analysis of polygonal tropical karst has been successful in assessing overall patterns of symmetry and otherwise (Williams, 1972, Day, 2004b), and using depth/diameter and width/length ratios of adjacent closed depressions and residual hills revealed nuances within type II cockpit karst landscapes (Day 1978, 1982), so similar approaches have promise in fengcong-fenglin differentiation. Fourier series analysis of Jamaican karst showed that terrain wavelengths could be used to uncover patterns of organization, including geologic influence, and distinguish between doline (type I) and cockpit (type II) landscapes (Brook and Hanson, 1991). Broadly, surface roughness may serve as a useful discriminator (Day, 1979, 1981; Day and Chenoweth, 2013a and 2013b), and differences in other variables, such as cave density, may also help in tower-cockpit differentiation (Zhu, 1982; Zhu et al. 1988), but these are not considered further here.

Despite the fact that utilizing DEMs and remote sensing to analyze landforms is well established in other branches of geomorphology (Bolch et al. 2005; Bubenzer and Bolten 2008), the application of DEMs in tropical karst geomorphology has remained challenging and immature due to unsolved issues. One issue is that the rugged topography blocks direct solar radiation, so satellite images are embedded with deep shadows, which cause image inconsistency because covered areas display reduced reflectance value compared to non-shadow areas with similar cover characteristics (Giles, 2001). Remote sensing software, such as ArcGIS and ERDAS IMAGINE tends to classify the shadow areas as a different category even if they have cover characteristics

similar to un-shadowed areas, such that the results of preliminary image classification do not represent the actual geometry of tower and cockpit karst. These issues have been addressed by topographic correction (Zhang et al. 2011) and spectral mixture analysis (Yue et al. 2010), which have achieved mitigation yet were time consuming and labor intensive in terms of cost and effect.

Another issue of geomorphologic mapping is that karst features with similar geomorphologic characteristics but different geologic histories may easily be misclassified (Ho 2011; Mylroie and Mylroie 2009; Purkis et al. 2010). Karst landforms can cause more confusion than those in other geological settings, and so image classification of surface karst landforms via remote sensing software should ideally be combined with field survey data (Day, 2004b).

Measurement of tower and cockpit karst is crucial to understand their morphological differences and to distinguish their evolutionary paths on a geochronological scale, and such measurement ultimately requires the use of RS and GIS (Day, 2004b). Digital Elevation Models (DEM) are critical in this context, playing a "...fundamental role in modulating earth surface and atmospheric processes" (Hutchinson and Gallant, 2000, p29). Remotely-sensed data, Digital Elevation Models and GIS techniques have been used to delineate karst features in the Cockpit Country of Jamaica (Chenoweth and Day 2001; Lyew-Ayee 2004; Lyew-Ayee et al. 2007; Fleurant et al. 2007, 2008) but these techniques have yet to be employed in discriminating between cockpit and tower karst.

The aim of this chapter is to classify tower karst and cockpit karst with greater accuracy and less confusion than hitherto, and this effort was attempted developing a novel method to categorize the two landscapes by utilizing the contours, slope and centroid derived

from the ASTER GLOBAL DEM (Digital Elevation Model). Classification accuracy was assessed through the verification of the corresponding region of interest exported on high resolution satellite imagery of Google Earth as the reference. Morphological indices were used to compare and contrast geomorphic variations using Object Based Image Analysis (OBIA).

2.2 Study area and data

The study area is located near Guilin, in the Guangxi Autonomous Region of China (Figure 3), which is renowned for its spectacular tower and cockpit karst landscape, and where the development of the two landscape styles is promoted by a unique combination of climatic, hydrological and geological conditions (Yuan, 1991, 2004; Zhu 1988).



Figure 3. Location of the study area

According to the Guilin Karst and Geological Structure report (1988), the geological framework of Guilin involves distinct basement and cover structures. The basement is characterized by NE-extending synclinoria composed of lower Paleozoic rocks, while the overlying cover structure is made up of Devonian and Carboniferous rocks, with Indosinian N-S-extending arcuate structures as the main framework, upon which are superimposed early Yanshanian NNE-trending Neocathaysian structures and late Yanshanian NW-trending structures. The protoliths of these tectonites are all carbonate rocks. Owing to the activity of karst hydrology in the later stages, the cementing material is often replaced by calcareous and argillaceous substances, forming metasomatic tectonites.

Under the influence of monsoons from the Indian and Western Pacific Oceans, the study area has pronounced dry and wet seasons, and 80 to 90% of total annual precipitation is received from May to October (Zhao, 1986). The climate in Guilin is a subtropical monsoon humid type (Liu 1991), with an annual average precipitation of 1873.6 mm and annual average temperature of 18.8°C (Yuan, 1992).

The major drainage system is that of the Li River, with both significant allogenic surface drainage and autogenic ground water contributions. The approximate catchment area upstream of Yangshuo is 5520 km² (Ru et al. 1988), with the estimated annual average recharge from the adjacent non-carbonate area being 41.9 x 10⁸ m³/year, and the average discharge flowing out from the basin being 67.8 x 10⁸ m³ yr⁻¹, giving an average regional recharge of 25.9 x 10⁸ m³ yr⁻¹ (Huang et al. 1988).

Spatially extensive, thick, pure and vertically uninterrupted Paleozoic age carbonate rocks provide the material base for the development of tower and cockpit karst in the

Guilin area (Zhu et.al. 1988), within a basin surrounded by distinct non-karst uplands: Yuechenglin to the north, Haiyangshan to the east, and Jiaqiaoling to the southwest. Within the karst landscape (Figure 4), tower karst accounts for 47% of the area and cockpit karst 53% (Zhu, 1982).

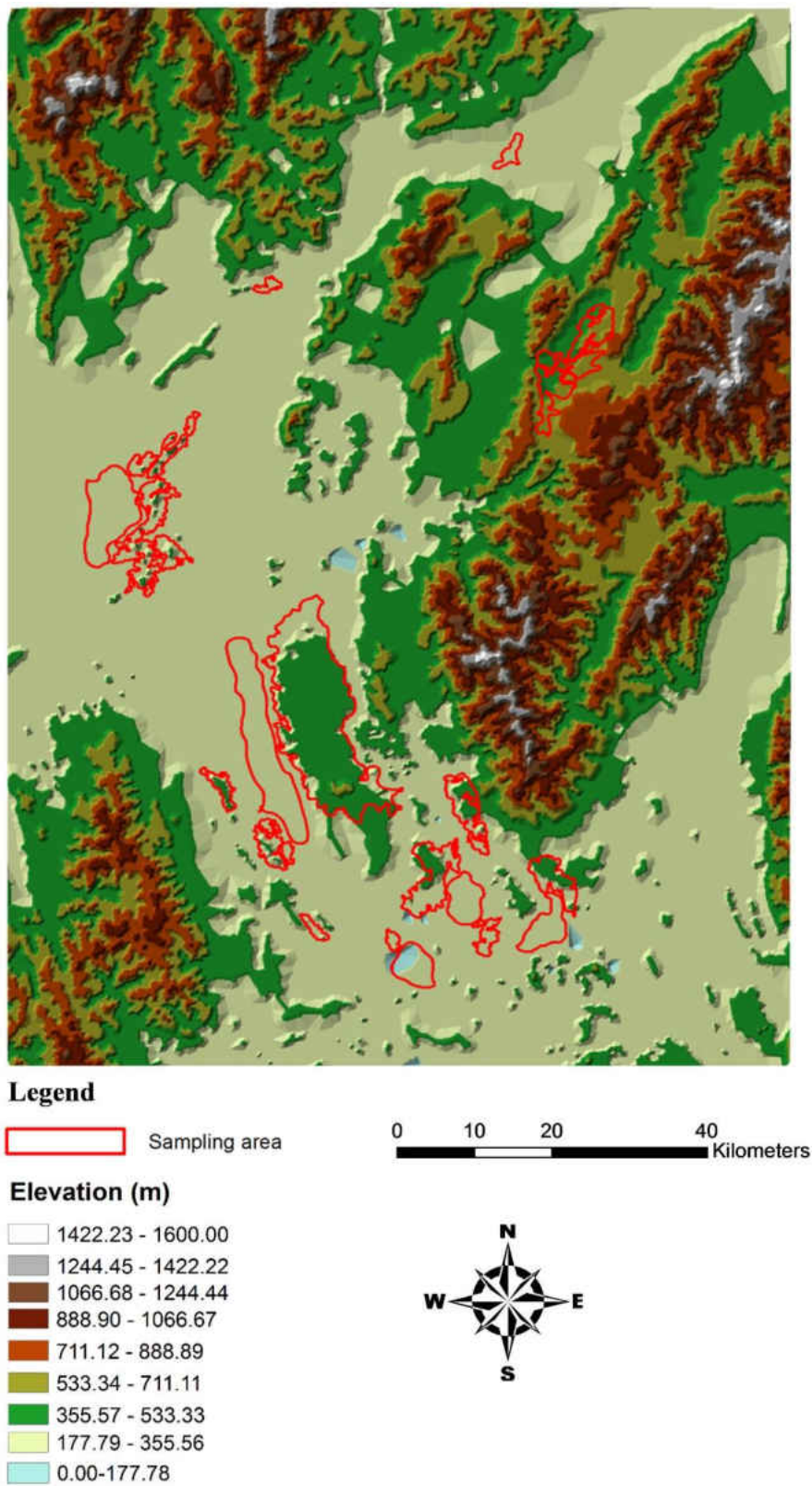


Figure 4. Distribution of fenglin/fengcong on the elevation map (Elevation unit: m)

2.3 Methodology

2.3.1 Main procedures

For geomorphological mapping, the ASTER Global Digital Elevation Model (GDEM) with 30 m spatial resolution was acquired from the website <http://gdem.ersdac.jspacesystems.or.jp/>. Related GIS data sets were acquired from the National Institute of Karst Geology in Guilin. All images and GIS data were projected with zone 49N and WGS 1984 datum.

Before implementing the model to classify tower karst and cockpit karst, several variables, including contour, centroid and slope were selected. Contour line delineates the actual hill profile at a certain altitude and can be used to identify the two landforms. Centroid reveals the number and position of the geometric center within the contour polygons, and therefore can be used to differentiate the tower and cockpit features. Slope represents the steepness of the hill and can eliminate unmatched hills with an appropriate threshold applied.

The ASTER GDEM data was first subset to the sampling area, and contour lines were extracted from the DEM at 10, 20, 30, 40 and 50 m intervals. Slope data was derived from the DEM and areas of >30 degrees were extracted because these are typical of tower and cockpit karst (Zhu, 1982). In order to use the contour lines which best represent the actual landforms, those with the smallest linear distance to the outer rim of the 30 degrees slope were selected. The closed contour lines were then converted to polygons, and the centroids of the polygons were then extracted. In differentiating tower and cockpit karst,

polygons of the former contain only one centroid, whereas cockpit polygons contain multiple centroids. After initial landform classification, the classification shape results were exported as KML files, and these files were referenced to Google Earth to assess how well the results match with the landforms on the high resolution imageries. Detailed procedures are displayed in Figure 5.

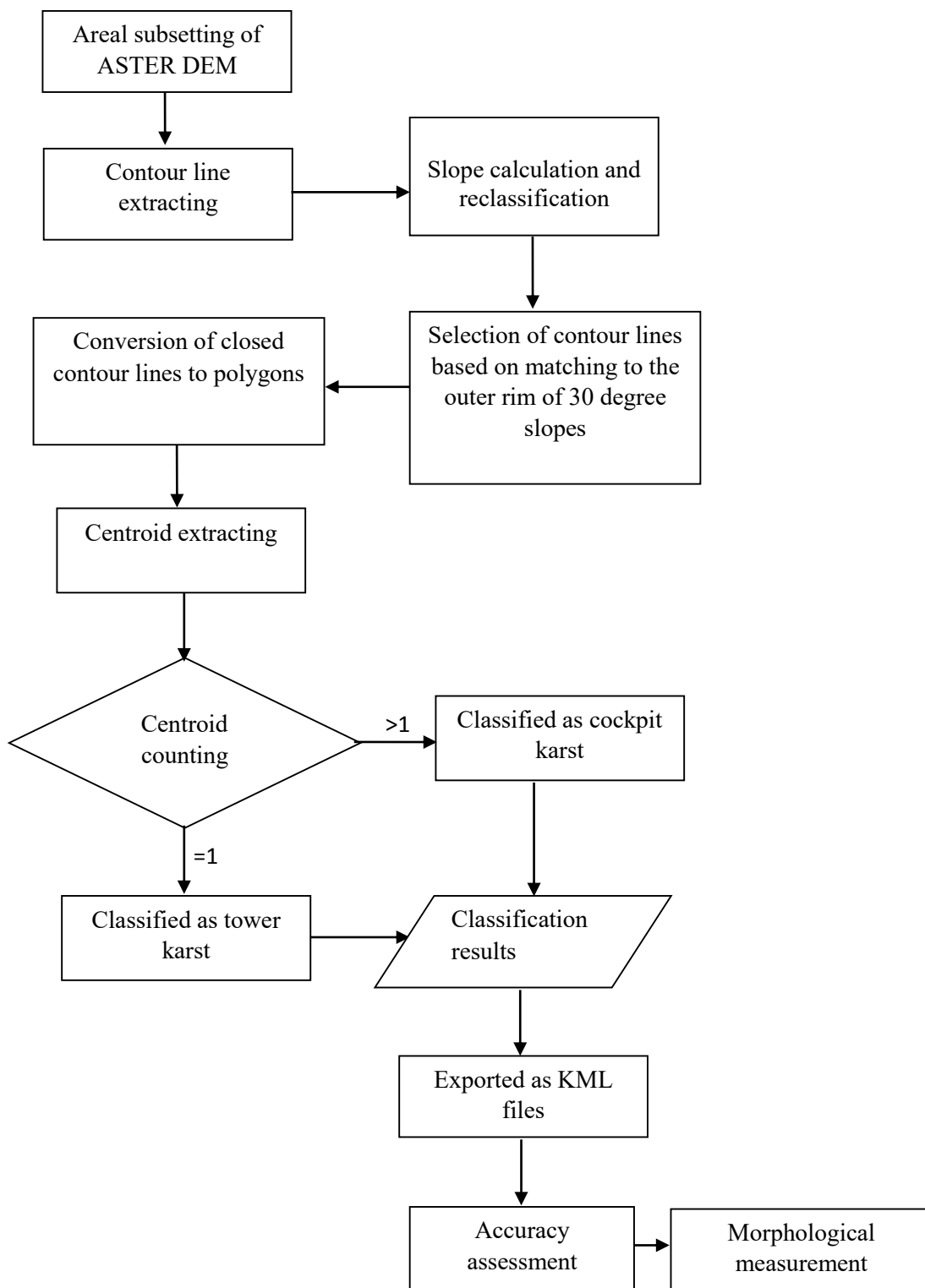


Figure 5. Flow chart of the methodology

2.3.2 Morphological measurement

After accuracy assessment, the classification results of shape files containing the original karst polygons were first converted to GeoTIFF format and then introduced into Trimble's eCognition Developer 64 8.7 software package to conduct object-based image analysis (OBIA). Image segmentation was performed by adopting 25 for the scale level and 0.5 for the color level. After segmentation, the new polygons generated by the software were checked and any sub-divided polygons sharing borders were manually merged with each other in order to maintain their shape identical to the original polygons. Area, length, length/width ratio, main direction, roundness and shape index were selected from the export result setting, then the new polygons containing the morphological attributes were exported.

In eCognition 8.7 software, both the asymmetry and length/width ratio feature describe the relative length of an image object compared to a regular polygon by approximating an ellipse. Since the asymmetry was less accurate than the length/width ratio (Trimble 2011), the ratio index was used for calculation. The main direction (the angle between the longer axis of polygons and North) was added to the polygon attributes to measure the direction of polygon orientation. In addition, the shape index (the ratio of the perimeter of the actual landform to the perimeter of a circle with the identical area) was also calculated to check the smoothness of the generated polygons.

2.4 Results and Discussion

2.4.1 Accuracy assessment

The accuracy assessment was based on the classification results, with Figure 6 showing an example from the sampling area after classification. One hundred polygons were selected randomly for tower karst and cockpit karst respectively and exported to Google Earth for validation (Figure 7).

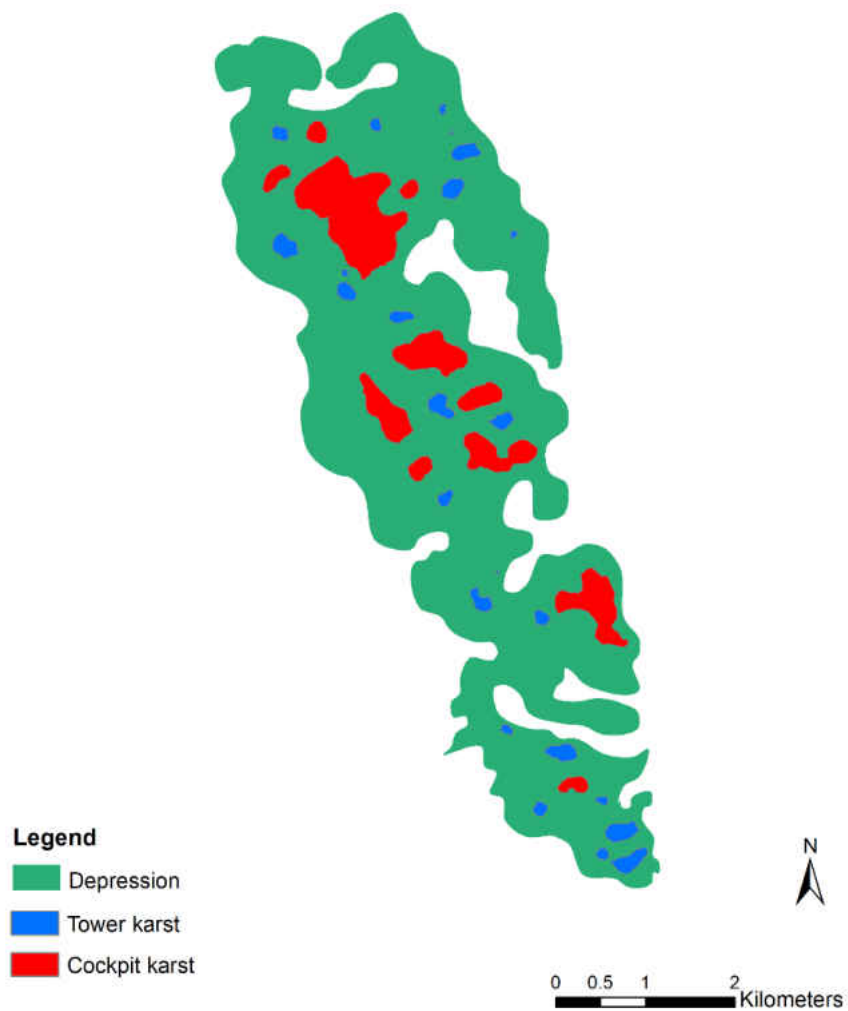


Figure 6. Example of karst landform classification



Figure 7. Verification of the classification result using Google Earth (Landscapes surrounded by blue circles are tower karst; landscapes surrounded by red circles are cockpit karst)

A confusion matrix (Kohavi and Provost, 1998) was used to report the classification accuracy (Table 1). The matrix contained actual results from Google earth and classified results from the proposed model. The column of tower and cockpit represent the number of correct and incorrect results in the corresponding category in the actual class, while the row of tower and cockpit represent the instances in the classified class. The producer's accuracy is calculated from the proportion of correct results in a specific column for the actual class. For example, the producer's accuracy for tower in the matrix is 74 out of (74+14), reaching 84.09%. Likewise, the user's accuracy is calculated from the proportion of correct results in a specific row for the classified class. As for the overall accuracy, it is calculated from the proportion of correctly classified results for both tower

and cockpit in the total of 200 sample points. The result indicated that, the accuracy measurement for both tower karst and cockpit karst attained better than 70% success in both the user's and producer's accuracy categories. The user's accuracy for cockpit was 86 %, which was higher than the tower. The relatively lower accuracy for tower is due to the geographical difference between tower karst and cockpit karst. Most cockpit karst in Guilin is located in rugged mountain areas with higher elevation and intervening depressions. By contrast, most tower karst is concentrated in the flat plain with lower elevation and relief with some sporadic distribution in the rugged mountain areas. Therefore, tower karst on the lower flat plain can be correctly classified by the contour lines with the lowest interval of 10 m, while those located in rugged mountain area are captured by the contour lines with interval larger 10 m and thus misclassified as cockpit karst. Another reason that may contribute to the misclassification is the mixture of tower and cockpit karst within the same area. Nevertheless, the overall accuracy in the sampling area reached 80%.

Table 1. Confusion matrix of tower and cockpit karst classification

Actual \ Classified	Tower	Cockpit	User's accuracy (%)
Tower karst	74	26	74
Cockpit karst	14	86	86
Producer's accuracy (%)	84.09	76.79	80

2.4.2 Morphological measurements

The results of the morphological measurements are shown in Table 2 and Figure 8, which indicate several aspects of geomorphic variation between tower karst and cockpit karst. First, the overall areas and the total perimeters of cockpit karst exceed those of tower karst. Second, the tower karst displays greater circularity than the cockpit karst, as

reflected in Figure 8, where roundness values in the tower karst are predominantly in the range between 0 and 0.5. Additionally, the longer axes of most tower features are oriented NE-SW to E-W, whereas the cockpits are mostly oriented in a broader arc NE-SW to SE-NW. Third, based on the comparison of shape indices, the towers are smoother shaped than the cockpits, with the cockpits having greater shape irregularity. Finally, the length/width ratios of both towers and cockpits is remarkably similar.

Table 2. Descriptive statistics of towers and cockpits

	Tower karst					
	Area (sq.m)	Perimeter (m)	Length/Width	Main Direction (degree)	Roundness	Shape index
Mean	33614.779	887.390	1.630	87.665	0.455	1.315
Standard Deviation	32216.878	483.897	0.468	46.849	0.274	0.142
Minimum	162	54	1	0.430	0	1.061
Maximum	161919	2538	3.251	176.884	1.807	1.7321
	Cockpit karst					
Mean	272949.674	4349.558	1.685	96.348	0.838	1.613
Standard Deviation	240668.444	4176.807	0.495	48.267	0.433	0.381
Minimum	196	56	1	0.730	0	1
Maximum	1006656	28336	3.367	177.284	1.731	2.933

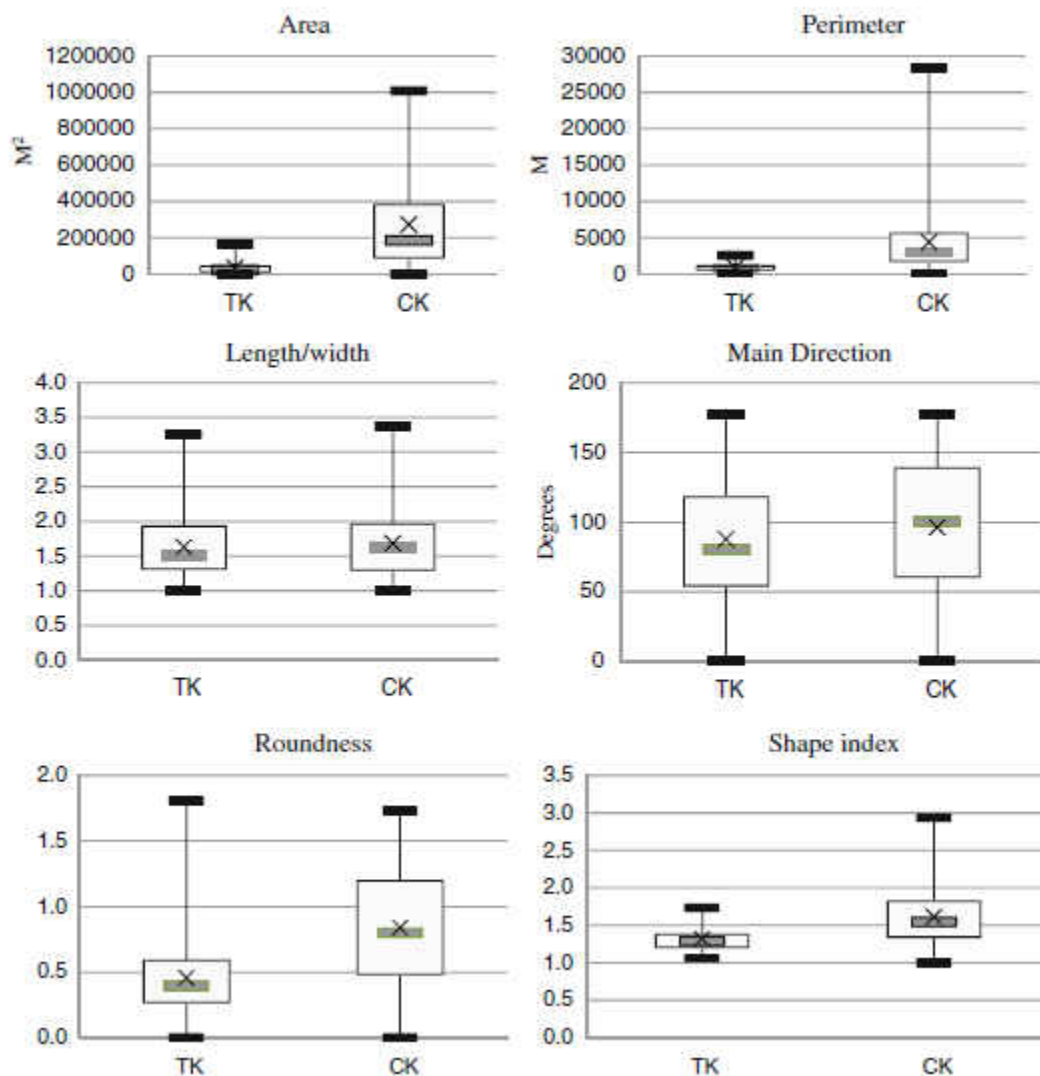


Figure 8. Box charts of six different morphological indices (TK: tower karst, CK: Cockpit karst)

2.4.3 Implication for geomorphologic classification and morphometric measurement

Liang and Xu (2013) utilized DEM to extract several variables such as area ratio, elevation, slope, and curvature to differentiate tower karst and cockpit karst in Guilin. They used a previous survey map as the reference to validate their classified results. The variables they selected are predominantly the most basic morphometric indices that can be easily extracted from DEM. Although these indices can differentiate tower and cockpit karst to some extent, they failed to provide detailed information about the spatial

distribution and dimension of the two landforms. On the other hand, their method of sampling and validation, although it initially sounds clear and correct, is problematic for several reasons. First, the samples collected from different tiles, no matter what scale they represent, are actually mixtures of tower and cockpit to some extents. Second, the reference map only provides general location but not accurate position of tower and cockpit karst. Third, the landforms have gone through a considerable change given the fast development of Guilin in the past decade, while the survey map was based on a survey conducted many years ago. Therefore, samples for morphometric analysis are not pure tower or cockpit type, and the survey map cannot provide reliable and accurate information for validation.

In contrast, the approach here not only explicitly classifies the tower and cockpit karst, but also delineates their actual outlines. As for the validation method, the most updated satellite imagery on Google Earth was used as the reference to validate the classified results. In addition, the object-based image analysis also produced accurate measurements of the two landforms that can reflect their morphometric and spatial properties.

2.5 Conclusion

Geomorphic classification of tower karst (fenglin) and cockpit karst (fengcong) using GIS and RS has been problematic because of shadows on the imagery. Topographic correction and spectral mixture analysis have provided some mitigation but they are time consuming, labor intensive, and incomplete. Here a combination of the contour lines, slopes, and centroids derived from ASTER DEM has been used to differentiate the karst landforms. The results suggest that using the DEM rather than optical sensor imagery in

karst surface extraction is a feasible way to avoid shadow problems and misclassification. This approach is also cost effective compared to topographic correction and spectral mixture analysis.

The extraction of morphological parameters of towers and cockpits was based on object-based image analysis, which provided a rapid and semi-automatic way to calculate geomorphic attributes of the two landform classes. Morphological analysis indicates that the towers and cockpits have significant morphometric variations in terms of area, perimeter, roundness, and shape. Main directions and length/width ratios are similar, perhaps warranting further study from a hydrogeologic perspective.

CHAPTER 3 INVESTIGATION OF VEGETATION ON SURFACE KARST USING TOPOGRAPHIC CORRECTION, SHADOW RETRIEVAL AND VEGETATION INDEX

3.1 Introduction

Karst landscape represents a fragile and heterogeneous environment constrained by local geology (Yuan and Zhang 2008; Parise, Wales, and Gutierrez 2009). Through the rapid dissolution of soluble rocks such as limestone and dolostone, tropical karst develops highly diversified surface landforms and subsurface caves. Among the different tropical karst geomorphological types, tower karst (fenglin) (Day and Tang, 2004) and cockpit karst (fengcong) (Day, 2004; Day and Chenoweth, 2013) are the two most spectacular and their interrelationships are critical to the understanding of tropical karst evolution as well as other surficial processes (Sweeting, 1972; Smart et al., 1986; Zhu, 1988; Yuan, 1991, 2004; Ford and Williams, 2007; Waltham, 2008).

Tropical karst landscapes, including those in tower karst and cockpit karst, are composed of a variety of land covers, including soil, bedrock, water, and vegetation. Extensive exposures of bedrock, however, are not a major land cover type in tropical karst area unless karst rocky desertification occurs in the appearance of a stone-desert-like landscape (Wang et al., 2004; Wang and Li, 2007). By contrast, vegetation can be classified as photosynthetic vegetation (PV) and non-photosynthetic vegetation (NPV). The former category includes plants that have green leaves, and the latter is referred as the plants that lack significant amount of chlorophyll (aboveground dead biomass, litter and wood) (Guerschman et al., 2009; Roberts et al., 1993).

Research into the linkages between vegetation and geomorphology, especially on hillslopes has developed significantly since the 1950s (Marston, 2010), but the focus has been unidirectional until recently (Viles, 1988). On the one hand, botanists and landscape ecologists tended to view vegetation as responsive to geographic processes and focused on the effect of topography on vegetation (Reinhardt et al., 2010). On the other hand, geomorphologists tended to treat vegetation as an independent variable that affects landforms and sediment at limited spatial–temporal scales (Renschler et al., 2007). Others (Harden, 2002; Marston et al., 2003; Keesstra et al., 2009), however, began to view the relationships between vegetation, geomorphology and landforms as dynamic, although the responses of vegetation to geomorphic processes need greater attention (Marston, 2010).

Traditional methods rely on field surveys of tropical karst vegetation type, structure, and on geomorphic measurement of hillslopes to assess association between vegetation and landform morphology. These methods are labor intensive and time consuming, making it

difficult to apply them at large geospatial scales (Wang and Li 2007). By contrast, remotely sensed data and related analysis techniques provide excellent data source at broad geographic scale and represent a cost effective way to extract vegetation cover information (Asner and Heidebrecht, 2003; Asner et al., 2005). Such approaches have been widely used in recent vegetation studies (Kim and Daigle 2011; Yue et al, 2013).

Vegetation indices have their own strengths and drawbacks in retrieving vegetation information. Indices such as the Normalized Difference Vegetation Index (NDVI) utilize spectral contrasts between chlorophyll absorption in the visible-red wavelength and cellulose scattering in the near-infrared wavelength (Tucker, 1979; Ustin et al., 2004) to identify green vegetation. Although the indices are not intrinsic bio-physical quantities of vegetation, they are widely used to assess vegetation vigor. However, their performance and suitability are place-dependent and determined by the sensitivity of the index to the characteristics of interest (Haboudane, Miller, and Pattey 2004). Nonetheless, NDVI is one of the most widely used methods of extracting vegetation information in most cases.

One significant issue with remote sensing of vegetation in tropical karst areas, particularly rugged ones, is the existence of shadows, which are cast on the ground, particularly on the sides of the hills due to the differentiation of direct illumination between sunny and shady slopes (Giles, 2001; Salvador et al.,2001; Yao and Zhang, 2006). Shadows not only cause reduction of the spectra of the shaded objects, but they also may lead to underestimation or misclassification of land cover classes (Dare, 2005; Hodgson et al. 2003; Weng, 2012).

There are several approaches to alleviate the influence of shadows on satellite imagery. Shadow detection and shadow restoration are considered in shadow correction algorithms.

For shadow detection, this process relies on the calculation of solar elevation, solar zenith and use of the Digital Elevation Model (DEM). In general, such algorithms include two basic types: thresholding and modelling (Liu and Yamazaki, 2012). To date, most shadow recognition techniques are based on setting a threshold value of the digital number such as a histogram to differentiate shadow regions from non-shadow regions. Pixels with digital number values smaller than the specific threshold are classified as shadow areas, while those higher than the threshold are classified as non-shadow areas. Modelling techniques, on the other hand, rely on specific mathematic concepts with related topographic information to simulate shadow regions (Shahtahmassebi et al. 2013). As an alternative approach, the Continuum Removal Technique was also applied in several studies (Zhou et al. 2014, Huang et al. 2004). This can normalize the spectra and allow a comparison of individual absorption from a common baseline (Kokaly, 2001). Several techniques have been proposed for removing shadows from the satellite imagery (Yang et al., 2007; Gao and Zhang, 2009). The most common approaches employ band ratio and vegetation indices (Riaño et al., 2003; Mather, 2004; Yesilnacar and Suzen, 2006; Jensen, 2007). Unfortunately, due to the loss of spectral resolution (Riaño et al., 2003), band ratios are nonlinear and subject to additive noise effects (Mather, 2004; Jensen, 2007). Alternative efforts in shadow restoration have been made using radiometric enhancement such as gamma correction (Nakajima et al., 2002), object-based approach (Zhan et al., 2005), linear-correlation (Sarabandi et al., 2004; Chen et al., 2007) and histogram matching (Sarabandi et al., 2004; Dare, 2005; Tsai, 2006). These methods all have their strengths and drawbacks as well. For instance, gamma correction uses a single gamma parameter for all pixels and hence ignores the existence of different backgrounds of

shadow areas (Zhan et al., 2005). Histogram matching can recover the digital values of a shadow region by matching its histogram to that in non-shadow region, but this approach is sensitive to the window size of the matched histogram (Shahtahmassebi et al 2013).

Few studies have adopted a comprehensive approach to shadow detection, vegetation restoration and vegetation index in rugged tropical karst terrains, so they have been unable to evaluate how vegetation correlates with hillslope topography. In many studies, shaded areas are left unclassified or simply classified as shadows (Shackelford and Davis, 2003), leading to misclassification of land cover information. Therefore, it could be advantageous to combine the aforementioned techniques together to investigate the topic. The aim of this chapter is to 1) Explore the potential of combining topographic correction and shadow restoration in the tower karst (fenglin) and cockpit karst (fengcong) of Guilin, China; 2) Calculate vegetation indices of tower/cockpit karst using NDVI and 3) Analyze the correlation between vegetation and topographic properties of tower karst and cockpit karst.

3.2 Study area and data

The study area is located near Guilin, in the Guangxi Autonomous Region of China (Figure 9), which is renowned for its spectacular tower and cockpit karst landscape, and where the development of the two landscape styles is promoted by a unique combination of climatic, hydrological and geological conditions (Yuan, 1991, 2004; Zhu 1988). A scene of cloud free Landsat ETM+ imagery on Oct 30, 2000 was acquired from the website of the Global Land Cover Faculty, University of Maryland (www.glcfc.umd.edu). An ASTER Global Digital Elevation Model with 30 meters resolution was acquired from

Earth Center (<http://gdem.ersdac.jspacesystems.or.jp/>). All data were projected using zone 49N and WGS 1984 datum.



Figure 9. Location of the study area

3.3 Methodology

3.3.1 Main procedure

The ASTER GDEM and the LANDSAT data were first subset to the study area, and the C-correction method (Teillet et al.1982) was applied for topographic correction. Shadow detection was achieved by using continuum removal, then shadow restoration was completed by collecting sample points from non-shadow aspects and using them to restore those samples on the shadow aspects. Classifying methods and results are based on previous study by Huang et al. (2014). The NDVI was then calculated based on the data after topographic correction and shadow restoration. NDVI and derived DEM products of elevation, aspect and slope were combined to analyze the correlation among them. The changes of Digital Number (DN) value in shadow areas before and after

correction were also compared to verify the change of NDVI value. Detailed procedures are displayed in Figure 10.

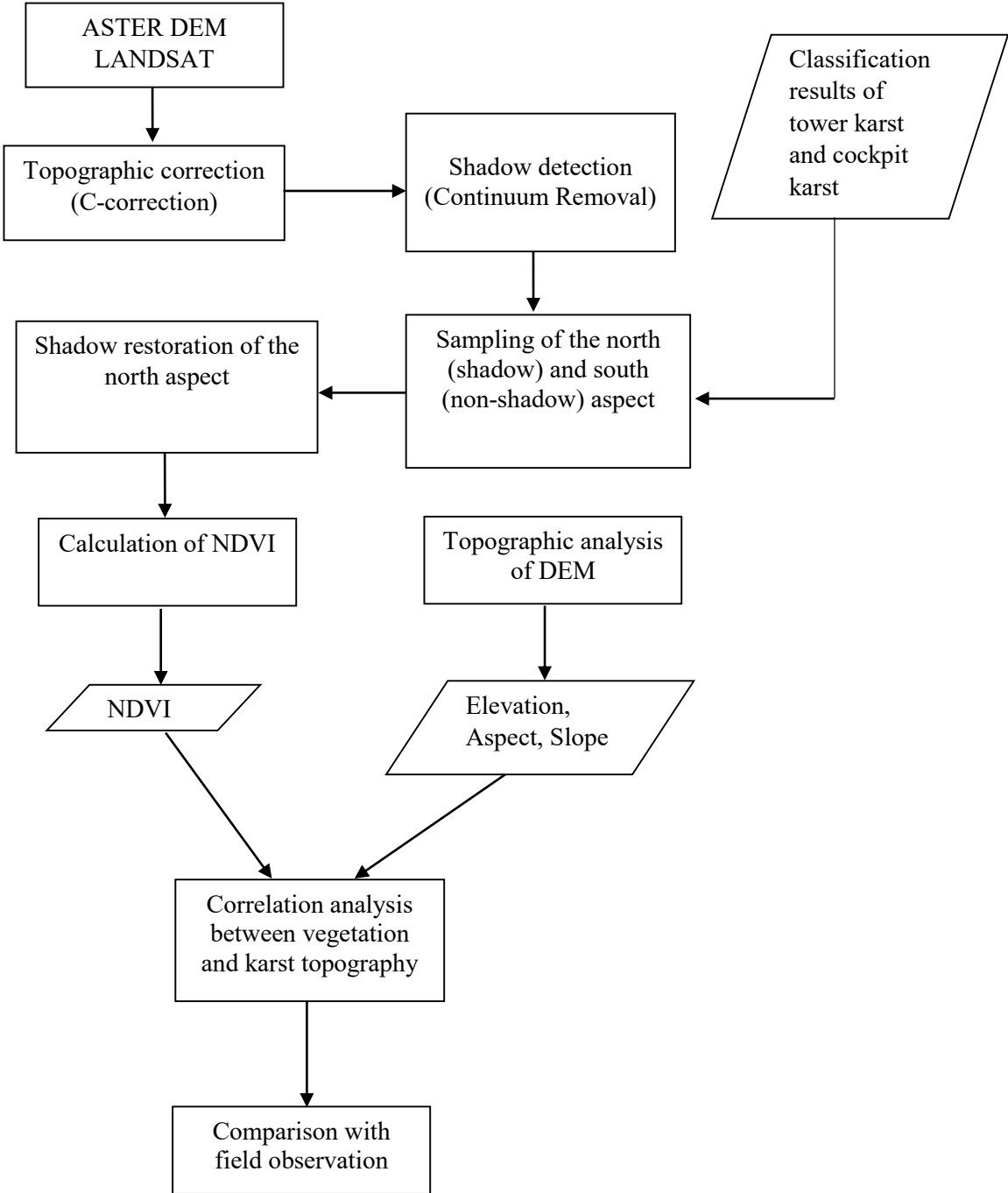


Figure 10. Methodology Flow chart

3.3.2 Topographic correction

In order to mitigate the influence of rugged topography, topographic correction was implemented by using the C-correction method (Teillet et al.1982), which is based on the most widely used cosine correction (Teillet et al.1982) with the assumption that the surface is Lambertian characteristic and capable of being a perfect diffuse reflector. For this reason, cosine correction can only correct illumination differences caused by orientation of the surface (Jones et al., 1988).

$$L_n = L \frac{\cos \theta}{\cos i} \quad (3.1)$$

$$\cos i = \cos \sigma * \cos \theta + \sin \sigma * \sin \theta * \cos(\beta - \omega) \quad (3.2)$$

Where L_n is the normalized reflectance, L is the uncorrected reflectance, θ is the solar zenith angle, i is the solar incidence angle, σ is the slope angle, β is the aspect angle, and ω is the solar azimuth angle.

The C-correction method is an extension of cosine correction by introducing the constant of C. There is a linear relationship between L (uncorrected reflectance) and $\cos i$ (cosine of the solar incidence angle).

$$L = a + b \cos i \quad (3.3)$$

$$C = \frac{a}{b} \quad (3.4)$$

Where a is the intercept and b is the regression slope.

The C-correction can be expressed as the following equation:

$$L_n = L \frac{\cos \theta + C}{\cos i + C}$$

3.3.3 Shadow detection

Shadow detection was achieved by applying a continuum removal method (Huang et al. 2004) to identify shadows that cannot be removed from previous topographic correction. The continuum removal reflectance (R_{cr}) can be calculated by dividing original actual reflectance value at a specific wavelength (R) for each band (λ_i) by the reflectance value (R_c) of the continuum line (convex hull) at the corresponding wavelength.

$$R_{cr(\lambda_i)} = \frac{R_{\lambda_i}}{R_c(\lambda_i)} \quad (3.6)$$

The image was first processed with continuum removal, then the shadows were extracted and exported for the next procedure.

3.3.4 Shadow restoration

In order to extract vegetation signature from karst hills, it is necessary to consider the topographic effect, specifically the shadows cast on the north sides where direct sunlight was blocked by the sunlit side of the hill. Each karst hill in the study area can be divided into shaded areas and non-shaded areas (sunlit slope). Using results from a previous study (Huang et al. 2014), samples were first collected from both sun-facing aspects and sun-shaded aspects. Then, mean and standard deviation of the pixels of each sample points were calculated. Digital values of sun-shaded slopes in the study area were corrected with the linear-correlation method (Nakajima et al., 2002; Sarabandi et al. 2004; Zhan et al., 2005; Chen et al., 2007).

$$DN_{recovered} = \frac{\sigma_{non-shadow}}{\sigma_{shadow}} (DN_{shadow} - \mu_{shadow}) + \mu_{non-shadow}$$

Where μ is the mean value and σ is the standard deviation.

3.3.5 Deriving the topographic indices from DEM

Topographic indices such as elevation, aspect and slope were derived from the Digital Elevation Model (DEM) respectively by using surface tools within the spatial analyst tools of ArcToolbox in ArcGIS. The aspect is an indicator of slope direction that represents the maximal change of rate downslope direction from each cell to its neighbors. The value of aspect is measured from North (0 degrees) to a clockwise round of due North (360 degrees).

3.3.6 Correlation analysis between corrected NDVI and karst topography

NDVI was calculated before and after image correction. Then, correlation analysis was conducted in order to investigate the relationship between corrected NDVI and topographic indices (elevation, aspect and slope) of tower karst and cockpit karst.

3.4 Results and Discussion

3.4.1 Result of topographic correction

Topographic correction using the C-correction method showed that shadows can be alleviated or even eliminated in lower relief regions, but in regions with greater local relief, shadows are still pronounced and need to be corrected (Figure 11).

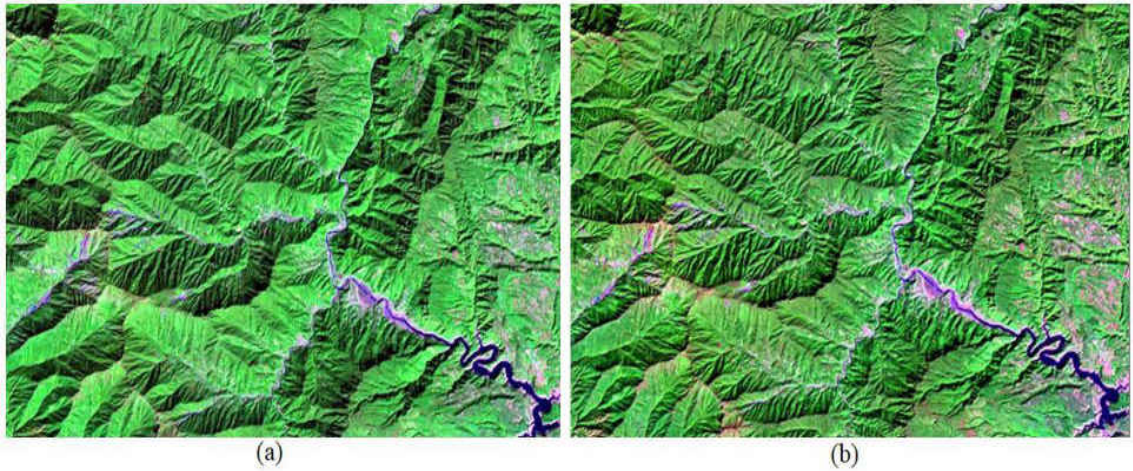


Figure 11. (a) Landsat-7 Imagery without topographic correction. (b) Landsat imagery with topographic correction (Band combination: RGB 642)

3.4.2 Result of Shadow Detection

The image was first processed with continuum removal, then the shadows were extracted and exported for the next procedure. The continuum removal technique detected most shadows and their shapes and positions match well with the actual presence on the image (Figure 12).

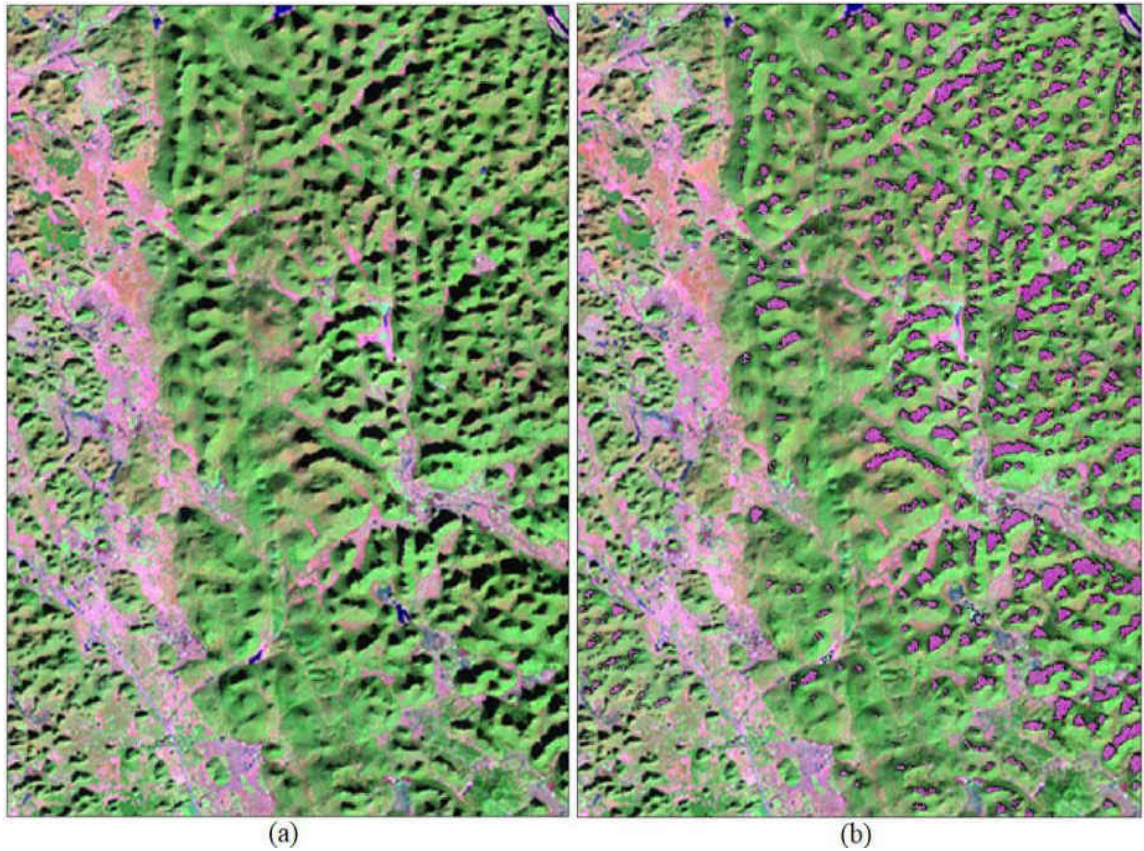


Figure 12. (a) Black shadows on the LANDSAT-7 Imagery. (b) Shadows detected on the LANDSAT-7 imagery with purple highlighted (Band combination: RGB 642)

3.4.3 Results of Shadow Restoration

Exactly 74,707 samples were collected from the shadow region on the north aspects and the same number of samples were collected from a 100-meter buffer of the north aspect within the south aspects. Mean and standard deviation of Band 4, Band 3 and NDVI before and after linear correction are calculated, respectively.

Table 3. Digital value (DN) statistics of samples from shadow areas and non-shadow areas

		Mean	Standard Deviation
Shadow areas	Band 4 before correction	27.049	12.572
	Band 4 after correction	57.306	18.298
	Band 3 before correction	28.264	5.424
	Band 3 after correction	38.054	8.578
	NDVI before correction	-0.056	0.141
	NDVI after correction	0.196	0.138
Non-shadow areas	Band 4	57.306	18.298
	Band 3	38.054	8.578
	NDVI	0.178	0.142

The advantage of using linear correction of DN values in shadow areas is that the corrected values achieved the same mean and standard deviation as those values from non-shadow areas (Table 3). In addition, Table 1 also showed that mean value of NDVI in shadow areas have been improved from -0.056 to 0.196, a level close to that in non-shadow areas (0.178). This will place the appropriate values for those dark pixels on the original NDVI image and provide better data for further analysis.

3.4.5 Comparison of the NDVI with topography between tower karst and cockpit

karst

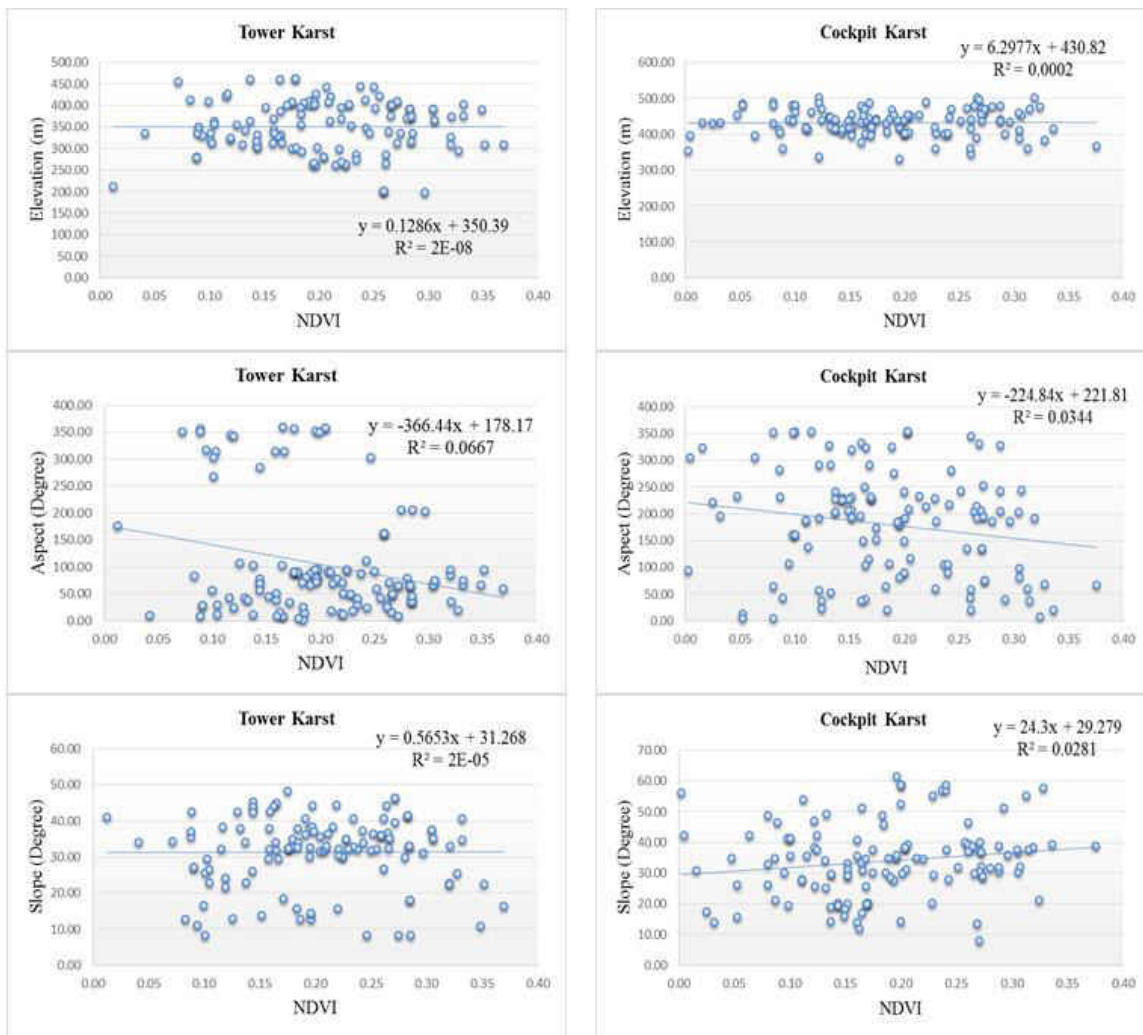


Figure 13. Scatterplots of NDVI and karst topography in tower karst and cockpit karst

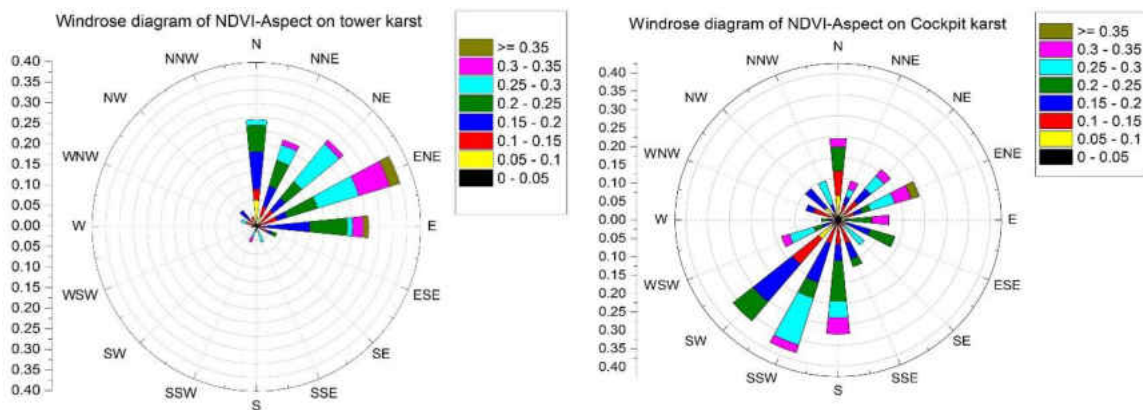


Figure 14. Windrose diagram of NDVI-Aspect on tower karst and cockpit karst

The correlations between vegetation coverage and karst topography were conducted based on the 128 sample points from both tower karst and cockpit karst (Figure 13). The low value of R square in all scatterplots suggests insignificant correlation between vegetation and variable topographic parameters. However, there is a clear distinction between the vegetation on tower karst and those in cockpit karst. For elevation, the distribution of vegetation for tower karst ranges from the 200m to 450m level (absolute elevation level) and such distributions are dispersed. By contrast, the distributions of vegetation for cockpit karst are relatively concentrated at the 400m-420m level with a slightly positive correlation. For aspects (Figure 14), vegetation on tower karst is more predominantly distributed in the north-east orientation (0-100 degree) and sporadically dispersed around 150 degrees. In particular, there is a pronounced absence at the south-south west direction (150-200 degrees), which is remarkable compared the tower karst in the study area (Figure 15). In the case of cockpit karst, the absence of vegetation within certain aspects is not apparent (as it is within tower karst) and the overall distribution is more dispersed. For slope, the vegetation coverage demonstrated similar distributions for both tower karst and cockpit karst, particularly in the slope of 30-40 degrees.



Figure 15. The absence of vegetation on the south aspect of tower karst (Photo taken during field survey of Guilin in Aug 2011)

3.5 Conclusion

Investigation of vegetation in tropical karst regions using GIS and RS has been problematic because of shadows on the imagery. Previous studies either ignored the shadows or primarily focused on non-shadow regions, leading to incomplete and inaccurate results. In order to address this issue, this study proposed a comprehensive approach of combining topographic correction, shadow retrieval and NDVI. The results suggest that vegetation distribution varies between tower karst, and cockpit karst and such differences correlate with the topographic characteristics of surface karst landforms. In particular, the under-representation of vegetation in the south-southwest aspect of tower karst was remarkable, and its overall distribution was less abundant and dispersed than in cockpit karst. As a practical approach, the proposed method has considerable

potential for retrieving vegetation information when combined with topographic correction and shadow restoration, which will provide solid bases for further geomorphic and hydrologic analysis.

CHAPTER 4 HYDROLOGIC CONTROLS ON DEVELOPING TOWER KARST AND COCKPIT KARST

4.1 Introduction

Hydrology plays an important role and defines the potential in developing karst landforms because the chemical dissolution of limestones and other soluble rocks require the interaction with water (Mangin, 1978). Hydrology is a major contributor to karst development, and it provides a significant perspective to understanding the characterization and evolution of karst landscapes (White, 2002). Karst hydrology is complex, however, because the characteristic multiple permeability, involving pores, fractures and conduits results in a wide range of permeabilities, rendering Darcy's law inapplicable in most cases (Ford et al. 1988). Therefore, soilless and water-scarce surface conditions often result from high permeability and require a unique methodology in hydrological analysis (LeGrand, 1973).

Jakucs (1977) defined the recharges to a karst zone from adjacent non-karstic areas as allogenic and those from within the karst as autogenic. This duality of recharge is an important component in understanding the hydrological controls over the development of tropical karst. Other work (McDonald, 1975) described the role of allogenic drainage in talus removal and the undermining of hillslope support in tower karst in Belize. Over time, as the drainage continues to improve around the tower, channel incision and

migration result in less active hillslope erosion, making the steep tower slopes more obscured at their bases. In his later work in Belize, McDonald (1979), stressed the importance of rivers and recommended that this agency should be explored more widely in interpreting karst landscape development, both within and beyond the tropics, including the classical karst areas. McDonald argued that rivers are important agents of geomorphic change, but are sometimes either not recognized or appear to be underestimated in many karst landscapes. Where rivers are present, their potential role in the geomorphic development of the karst landforms should be thoroughly evaluated, including detailed field studies and the consideration of geological and sedimentological evidence.

Footcaves at the bases of towers were identified by McDonald as an important cause of steep flanks, eventual collapse and elimination of towers. They are associated with surface and shallow ground waters active both in chemical processes and in “normal” stream corrasion (McDonald and Twidale, 2011). Regardless of whether the towers stand in isolation or in massifs, they are commonly riddled with caves and other voids (Jennings, 1976). In humid tropical regions, where tower karst areas are traversed by rivers flowing from non-karst areas, coarse detritus carried by the river will serve as the tool of corrasion and undercut the bases of the towers (McDonald and Twidale, 2011). McDonald (1975, 1976a, 1976b, 1979a, 1979b; McDonald and Ley, 1985) reported that in fenglin karst in Sarawak, Sulawesi, Belize, and Tabasco rivers in the monsoon/ wet season flood the plains, making karst towers islands in ephemeral lakes. In addition, McDonald also noted that sand and coarse fluvial debris in those areas had been transported and deposited on valley floors and plains, provided that the area is either

close enough to the watertable for rivers and streams to remain at the surface, particularly where they enter karst areas from a non-karst terrain. Such seasonal variation of allogenic recharge was confirmed by Palmer (1975), who found this to be the case in a maze cave bordering a non-karst catchment with high relief.

In addition to mechanical affects, allogenic recharge and internal runoff have powerful undercutting capabilities because they are generally under-saturated with respect to carbonate minerals and can initiate or accelerate the dissolution process in the carbonate aquifer (White, 1988). As Miller (1987, p. **) stated in the case of Guatemala, “Fully-integrated streams from non-carbonate highland appear to have been the primary factor in developing the surface karst of the area; disaggregation of a fluvio-karst surface has produced classic cockpit karst...”

Williams (1985) described the role of allogenic recharge in areas of pure, dense limestone and a humid warm climate as leading to the formation of point recharge depressions. Guilin seems to be an extreme example and, according to Yuan (1985) and Williams (1980), tower karst in Guilin mainly occurs where surface runoff concurs with shallow depth water-tables, whereas cockpit karst occurs where the water-table is below the bottom of any enclosed basin. Using this comparison, Yuan (1985) concluded that tower karst is not an icon of later phases of evolution and cockpit karst is not necessarily an initial stage, and therefore a parallel rather than sequential model of development deserves deep reconsideration.

Karst aquifers serve as intermediate layers that link surface runoff and groundwater, allowing the surface water to go underground through infiltration (Ford et al. 1988). They also represent valuable water resource for residents living in karst zones. Nonetheless,

since water contained in the aquifer may exist in both the vadose and the phreatic zones, it may be difficult to access from the surface, and is always vulnerable to contamination (Goldscheider and Ravbar, 2007).

One of the major challenges in karst groundwater modeling is the potential coexistence of both Darcyian and non-Darcyian flow in the aquifer. Groundwater flow in pores, small fractures and tight fissures is slow and may be approximated by Darcy's law, but flow in open fissures, large conduits and caves is turbulent (Kincaid, 2004), rendering Darcy's law inapplicable (Faulkner et al 2009). As a result, applying popular models such as MODFLOW (Harbaugh, 2005) and MT3D will not guarantee correct results (Zheng and Wang, 1999) that can be compared with field observation.

There are several approaches to this issue. One is to use observational data from wells or pumping sites as references to generate hydrographs (Bonacci 1982 and 1995), although other hydrologists argue that wells are independent of conduits, and thus cannot represent the hydrology of karst aquifers (Ford and Williams 1989; Jeannin and Sauter 1998; Smart 1999). Another approach is to use lumped models that assume the aquifer is a "black box" and predict its behavior by combining systematic inputs, outputs and transfer functions (Martínez-Santos, 2010). Efforts to establish correlations between recharge, transfer and discharge, however, neglect due consideration of the physics of groundwater flow (Zhang et al., 1996 and Fleury et al., 2007). Another approach, the distributed model, is based on the assumption that there is an equivalent porous medium in the aquifer, which requires detailed information to render the hydrologic data with spatially coordinated elements (Scanlon et al., 2003). Distributed models can also be elaborated by coupling Darcyian and non-Darcyian flow (Stokes or Navier–Stokes systems) in the same model, but the

simulations rely heavily on detailed pre-investigation and expert knowledge of the karst conduits and fissures within the aquifer (Doummar et al 2012). Therefore, such applications are limited to small areas (Guo and Chen, 2006).

Solute transport mechanisms depend on the hydraulic behavior of the epikarst zone, the flow out of which is a major factor that controls solute transport to the phreatic zone in the aquifer. In particular, the hydraulic response of karst aquifers to storm events is important to understanding solute transport mechanisms (Trček, 2008).

Solute transport in karst conduits is typically accomplished by rapid, turbulent flows within a short period of time, while models of solute transport in surface water flow can be determined empirically from quantitative ground water tracing studies (Field, 1997).

Few studies, have adopted a comprehensive approach to estimating the hydrological control of tropical karst by combing groundwater modeling, solute transport modeling and geographical analysis. Therefore, it could be advantageous to combine the aforementioned techniques together to investigate the topic. The aim of this chapter is to 1) explore the water regime in the tower karst (fenglin) and cockpit karst (fengcong) of Guilin, China; 2) combine both groundwater and solute transport models in the analysis, and 3) estimate the bicarbonate concentration dynamics for both fenglin and fengcong.

4.2 Study area and data

The study area is located near Guilin, in the Guangxi Autonomous Region of China (Figure 16), which is renowned for its spectacular tower and cockpit karst landscape, and

where the development of the two landscape styles is promoted by a unique combination of climatic, hydrological and geological conditions (Yuan, 1991, 2004; Zhu 1988).

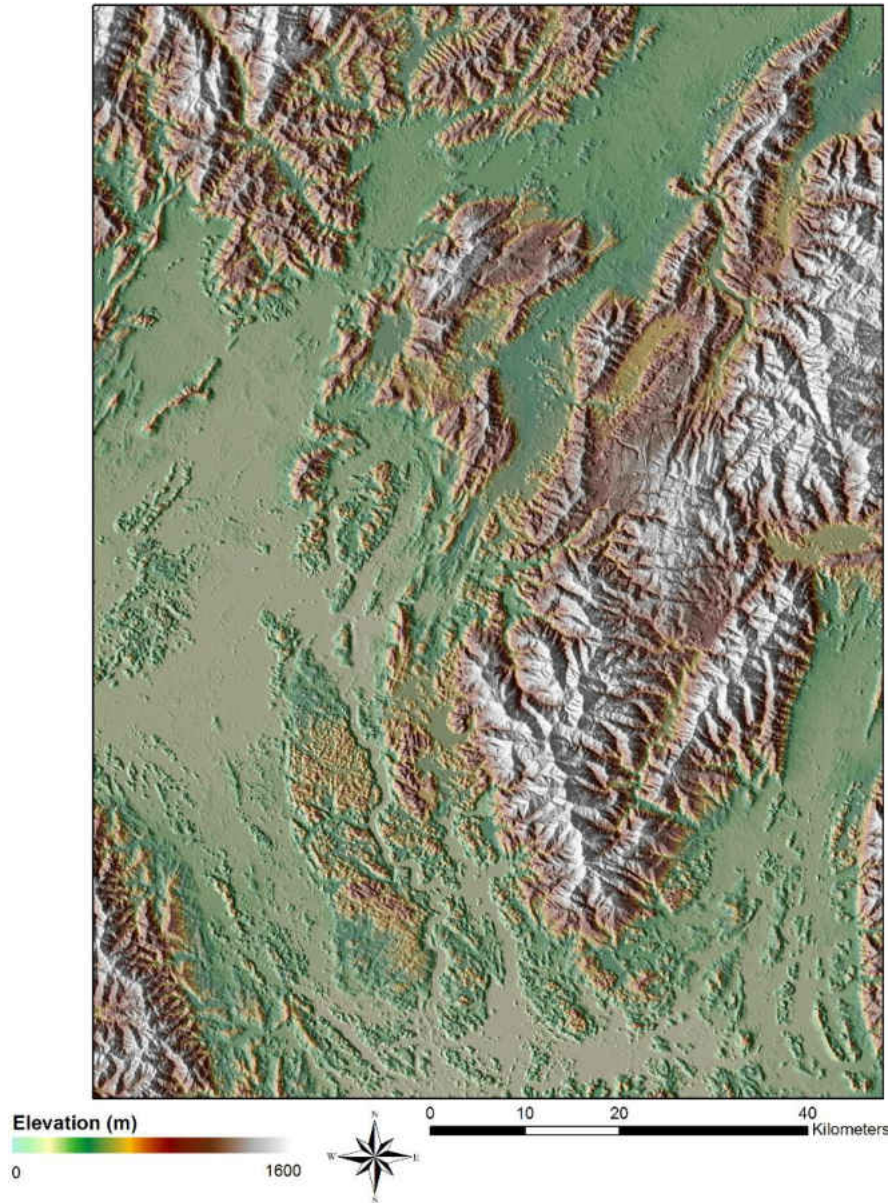


Figure 16. Study area elevation map

Under the influence of monsoons from the Indian and Western Pacific Oceans, the study area has pronounced dry and wet seasons, and 80 to 90% of total annual precipitation is received from May to October (Zhao, 1986). The climate in Guilin is a subtropical

monsoon humid type (Liu 1991), with an annual average precipitation of 1873.6 mm (Figure 17), annual average temperature of 18.8°C (Figure 18), and annual average runoff of 124 m³/s (Figure 19).

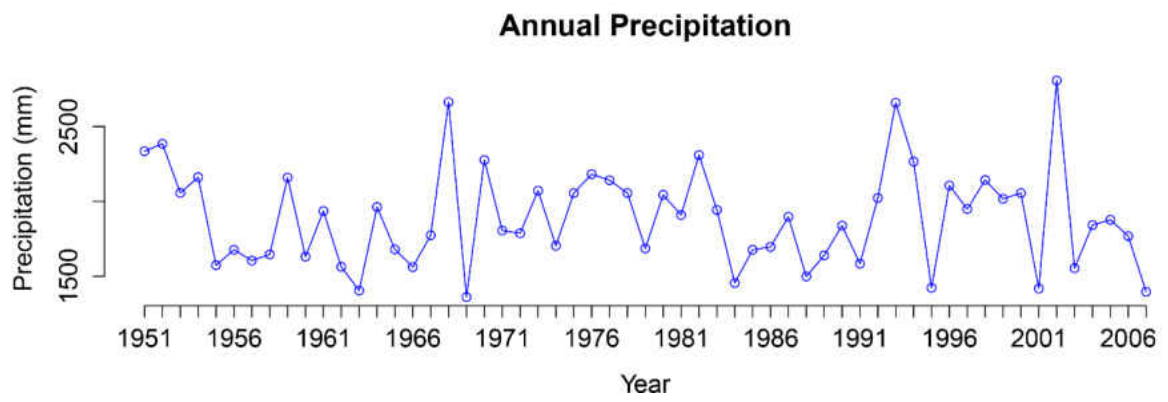


Figure 17. Annual precipitation of the study area

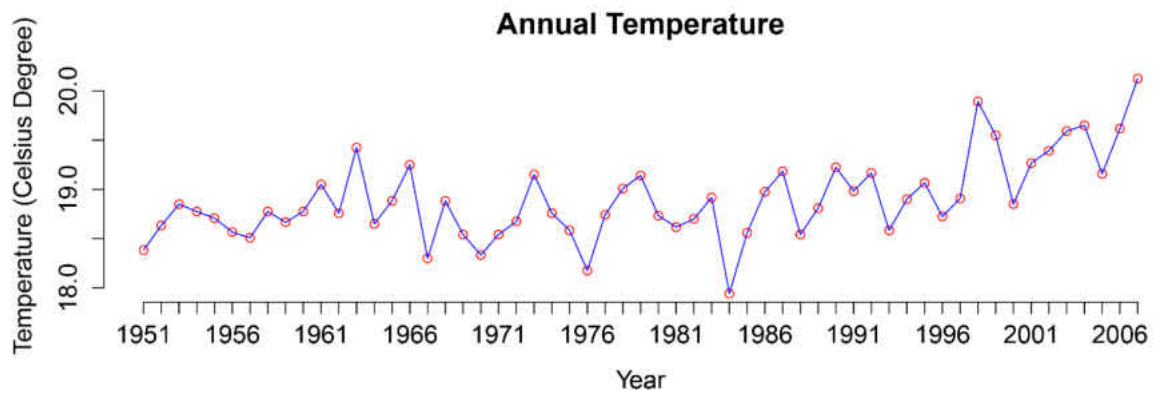


Figure 18. Annual temperature of the study area

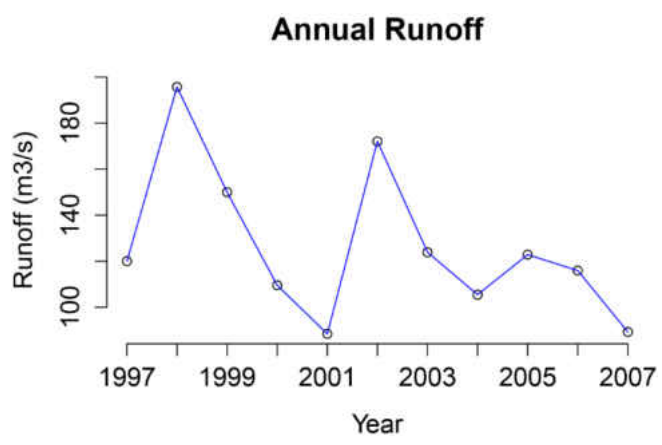


Figure 19. Annual runoff of the study area

The soil sample data of sampling sites was acquired from Harmonized World Soil Database (HWSD) viewer developed by the International Institute for Applied Systems Analysis (IIASA). Bicarbonate concentration of wells and springs across the study area was acquired from previous survey (Guilin Institute of Karst Geology, 1988)

4.3 Methodology

4.3.1 Watershed Delineation

There are several steps in the process of watershed delineation (Figure 20), including the following:

1. Create a DEM without depressions

The first step in watershed delineation is to create a DEM (Digital Elevation Model) without depressions. This can be achieved by filling sink cells and areas of internal drainage in the original DEM data.

2. Calculate flow direction

Flow direction is calculated from each cell to its steepest downslope neighbors in the format of a raster file.

3. Calculate flow accumulation

The calculation is conducted by creating accumulated flow to each cell during the process, in which relevant streams, stream links and stream order were also generated. A threshold of 5000 was applied to the stream network in order to create the streams in every pixel.

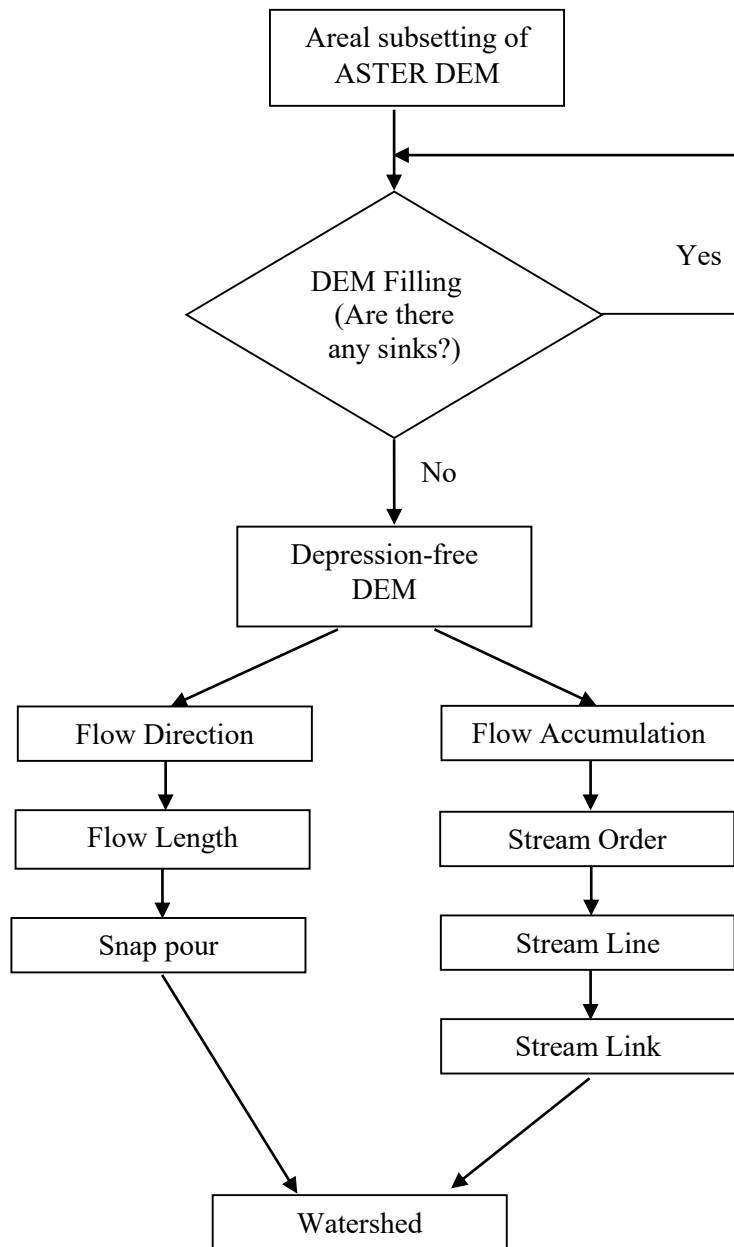


Figure 20. Methodology of delineating of watershed

4.3.2 Hydrological chart in the study area

The research regards fenglin and fengcong as subsystems in the study area, each of which has its own hydrological inputs and outputs. The fengcong system has a thick vadose zone underground and the allogenic flow from non karst areas can be ignored due to its extremely small volume (see Figure 21). The fenglin system, on the other hand has multiple inputs (including allogenic flow) and multiple outputs in the scheme (see Figure 22). It should be noted that the fenglin system involves longer response time than the fengcong system because of its multiple inputs.

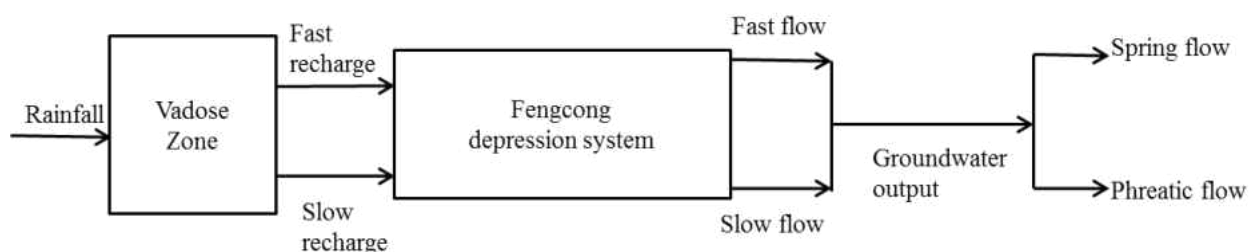


Figure 21. Hydrological chart of fengcong depression system (After Guilin karst geology, 1988)

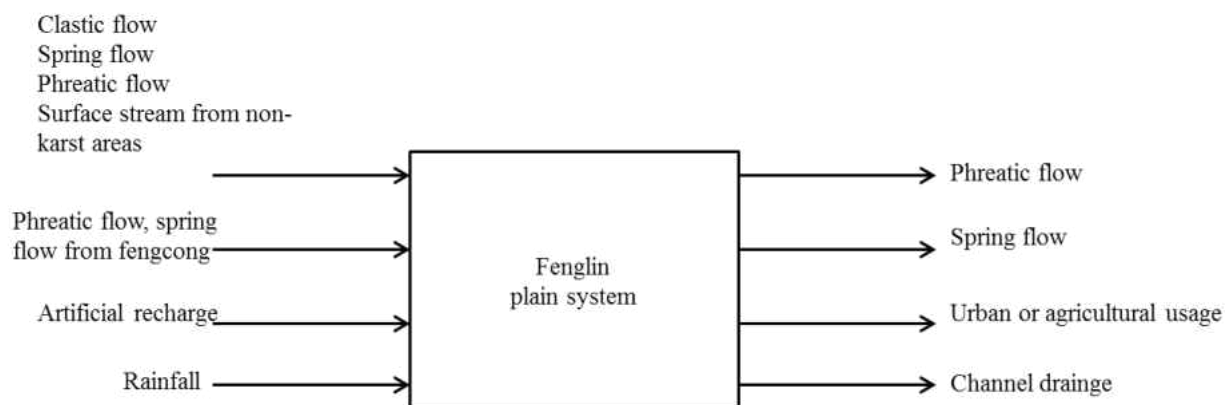


Figure 22. Hydrological chart of fenglin plain system (After Guilin karst geology, 1988)

Comparison of annual rainfall and annual runoff indicated that the groundwater recharge has significant contribution in the total water budget, so solute transport calculation in the study will be primarily focused on the groundwater part (Figure 23).

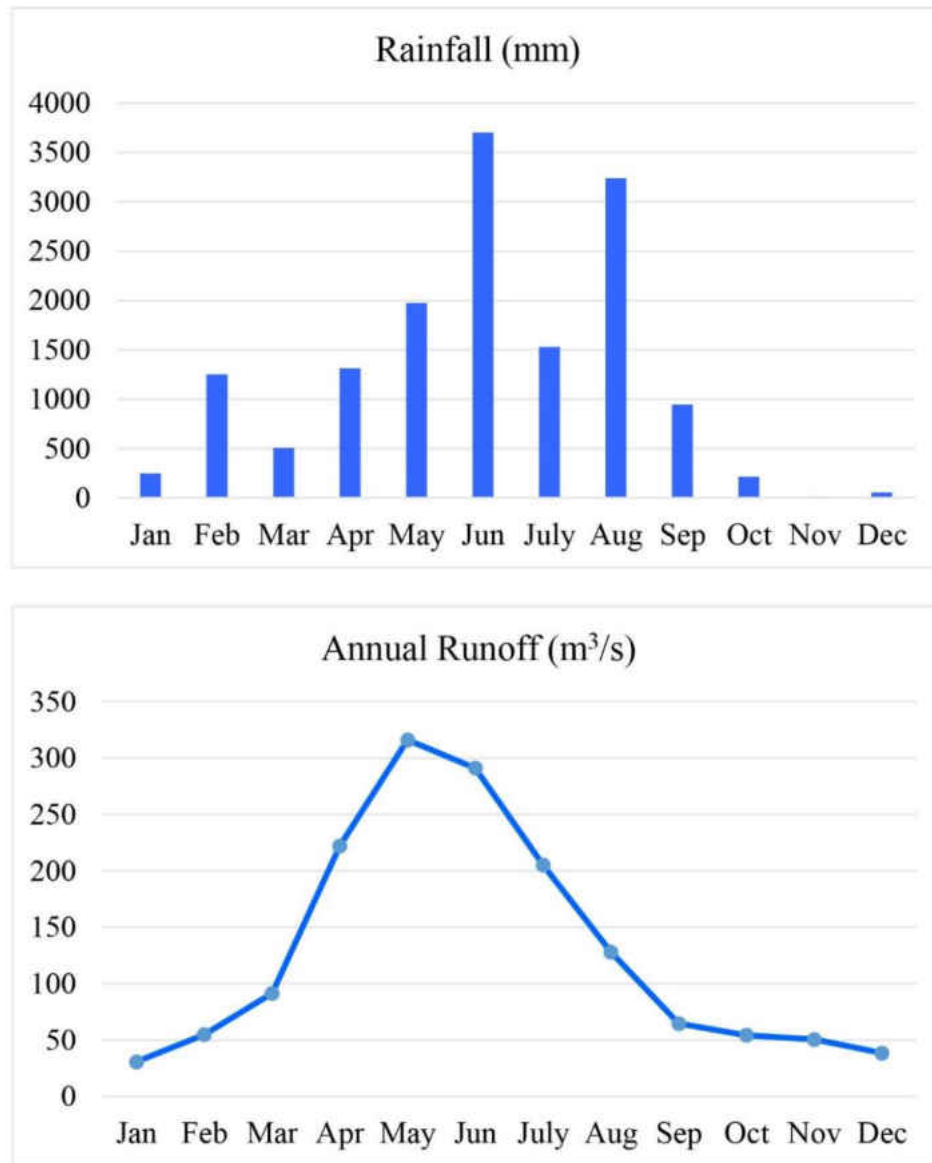


Figure 23. Comparison of Annual Rainfall and Annual Runoff

4.3.3 Groundwater model and solute transport model

Richard's equation was used for the groundwater flow in the one dimensional partially saturated porous media

$$\frac{\partial \theta}{\partial t} = \frac{\partial}{\partial z} \left[K \left(\frac{\partial h}{\partial z} + 1 \right) \right] - Q \quad (4.1)$$

Where h is the hydraulic head (L), θ is the water content (L^3L^{-3}), K is the hydraulic conductivity (LT^{-1}), t is time (T), z is the spatial coordinate (L), and Q is the sink-source term (T^{-1}).

Due to the uneven nature of groundwater media, two different formulas (McDonald and Harbaugh, 1988) were used in the two dimensional calculation. For a two dimensional confined aquifer, the formula is

$$\frac{\partial}{\partial x} \left[K_x(h-b) \frac{\partial h}{\partial x} \right] + \frac{\partial}{\partial y} \left[K_y(h-b) \frac{\partial h}{\partial y} \right] - W = S \frac{\partial y}{\partial t} \quad (4.2)$$

$$T = k(h-b)$$

In the scenario of a two dimensional unconfined aquifer, the formula is

$$\frac{\partial}{\partial x} (hK_x \frac{\partial h}{\partial x}) + \frac{\partial}{\partial y} (hK_y \frac{\partial h}{\partial y}) - W = S \frac{\partial y}{\partial t} \quad (4.3)$$

Where h is the hydraulic head, k_x and k_y are the principal components of the hydraulic conductivity tensor, T is the transmissivity tensor, b is the elevation of the bottom of the aquifer, W is the volumetric flux source or sinks of water, S is the specific storage of aquifer, t is time.

The solute transport model for bicarbonate ion (Šimůnek and Suarez, 1994) was used in the bicarbonate estimation.

$$\frac{\partial(\theta c_k)}{\partial t} + \rho \frac{\partial \bar{c}_k}{\partial t} + \rho \frac{\partial \hat{c}_k}{\partial t} = \frac{\partial}{\partial x_i} (\theta D_{ij} \frac{\partial c_k}{\partial x_j} - q_i c_k) \quad (4.4)$$

$$k = 1, 2, \dots, N_c$$

Where c_k is the total dissolved concentration of the aqueous component k (ML^{-3}), \bar{c}_k is the total adsorbed concentration of the aqueous component k (MM^{-1}), \hat{c}_k is the total precipitated concentration of the aqueous component k (MM^{-1}), ρ is the bulk density of the medium (ML^{-3}), D_{ij} is the effective dispersion coefficient tensor (L^2T^{-1}), q_i is the volumetric flux (LT^{-1}), and N_c is the number of aqueous components.

4.3.4 Estimation of bicarbonate concentration

In order to estimate the bicarbonate concentration at sample sites from chapter 2 (geomorphic differentiation of fenglin and fengcong), water table gradients in the study area were calculated from the ASTER DEM, then the flow path consisting of seepage velocity and direction was calculated. The solute transport model was then applied to the flow path for the estimation (Figure 24). Various observation results from previous survey (Guilin karst geology, 1988) were used as initial injection point to predict the bicarbonate content in the study area.

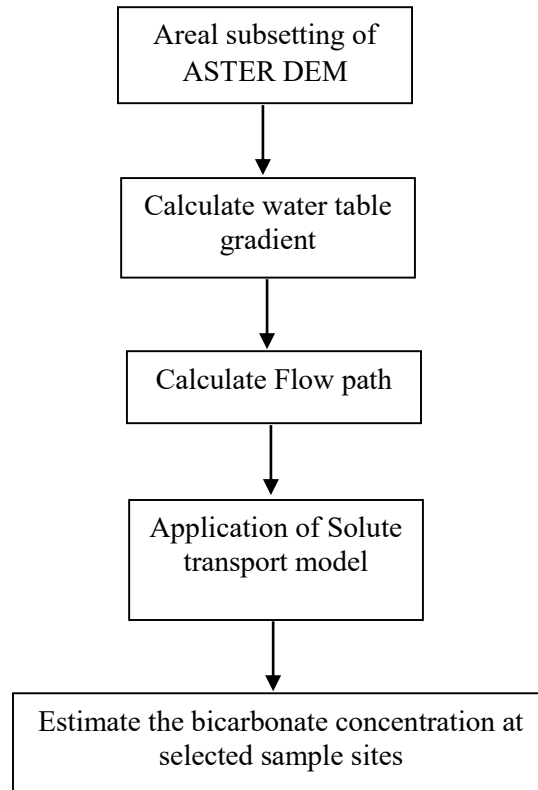


Figure 24. Bicarbonate estimation from solute transport model

4.4 Results and Discussion

According to the inquiry from the Harmonized World Soil Database (HWSD), the three major soil types in the study area are Haplic Luvisols, Dystric Regosols and Cumulic Anthrosols, with mixed rock outcrops (Figure 25). Since most of the sample area is located in the Luvisols zone, Regosols and Anthrosols are not considered in the study.

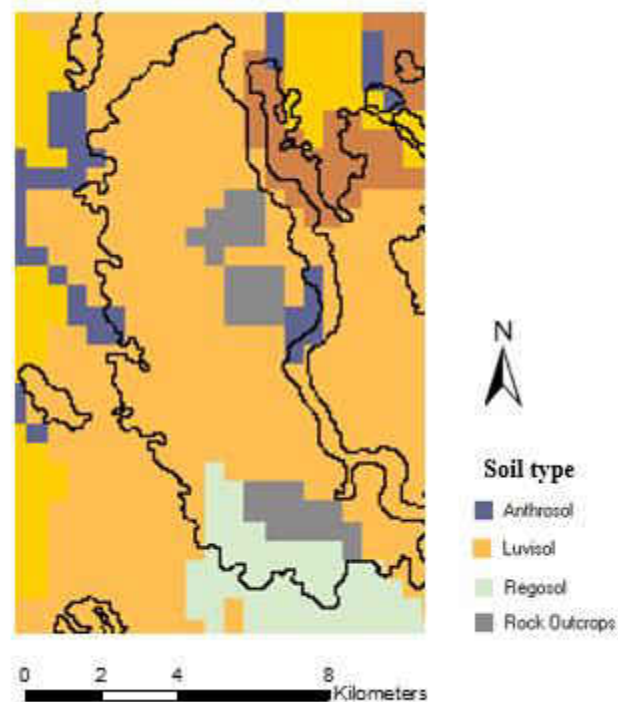


Figure 25. Soil types in the study area

Figure 26 demonstrates the pressure distribution at different depths of the sampling sites. The vertical axis represents the depth of sample sites and the horizontal axis represents the pressure head. The total time for the pressure simulation is 10 days with 5 intervals. The initial blue line at zero seconds reaches the depth of 7 cm. As time progresses, surface runoff penetrates to deeper depths and develops its own pressure profile, with associated permeability.

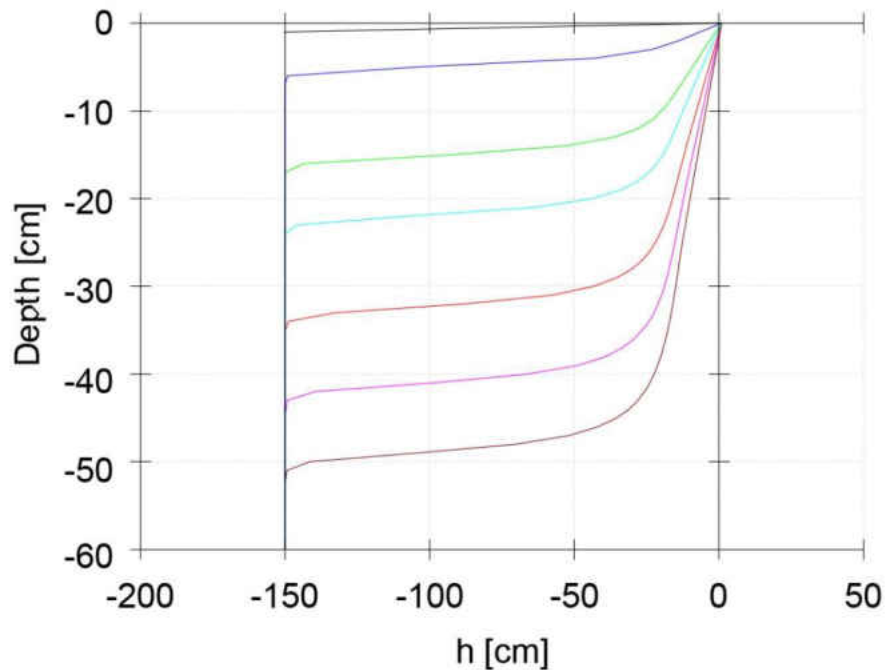


Figure 26. Distribution of pressure (h) at different depth of sample sites

In figure 27, the simulation of bicarbonate transport follows the same time frame of ten days (864,000 seconds). Runoff carrying bicarbonates infiltrates underground through variably saturated porous media and the solute transport process is much slower than in surface water. The ultimate concentration of bicarbonate after the elapse of 10 days ranges between 0.2 and 0.3 kg/m^3 (200-300 mg/l). The figure suggests that Darcyian flow may also exist in the transport environment, but its roles in regulating groundwater is constrained to limited fractions of the aquifer.

The result of bicarbonate concentration simulation is based on 100 samples and suggests that, as might be expected, autogenic recharge from the carbonate area (light purple zone of Figure 28) has a relatively higher concentration of bicarbonate, while the input from the non-carbonate zone (rugged terrain with heavy shadows with blue and dark purple) demonstrates lower concentrations of bicarbonate.

Solute transport of bicarbonate (kg/m^3)
 (Time = 8.64×10^5 seconds, arrows indicate major vector directions of Darcy's flow)

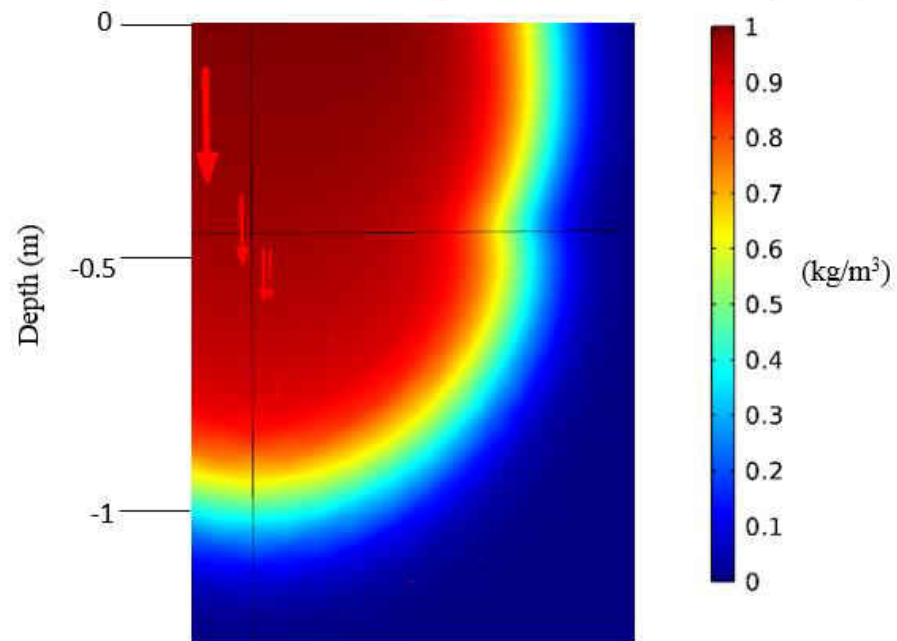


Figure 27. Solute transport of bicarbonate

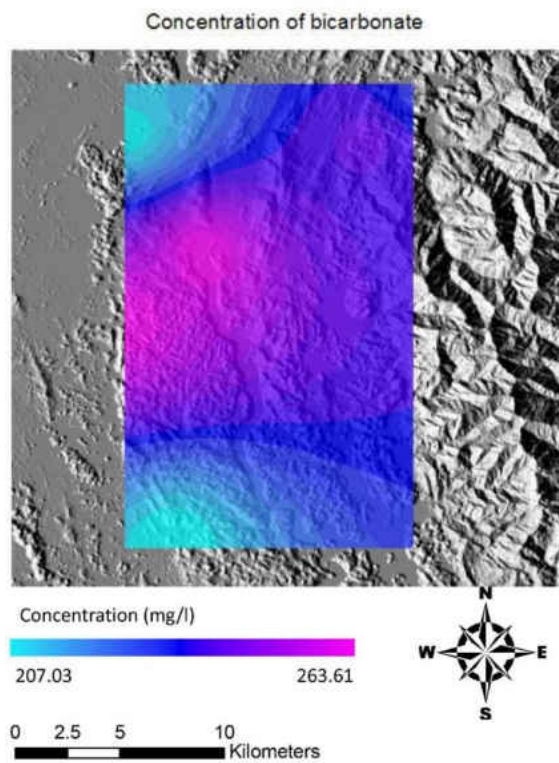


Figure 28. Bicarbonate Concentration in the study area

4.5 Conclusion

Estimating the hydrological control on tropical karst is a big challenge due to the heterogeneous nature of the porous aquifer. The study combined the ground water model and solute transport model to estimate bicarbonate concentration. The results suggest that, as would be anticipated, the permeabilities of karst aquifers in the study area vary in depth, and that there are higher levels of bicarbonate ions within the karst area than in the non-carbonate area.

CHAPTER 5 EDGE EFFECT

5.1 Introduction

Edge effects are widely acknowledged phenomena in ecology, typically occurring in transitional sites where different habitats intersect. In particular, they occur as several hundred meters-wide transition zones where adjacent but distinct ecosystems interact with each other (Murcia, 1995) or where “natural” ecosystems abut adjacent disturbed or developed land (Andren, 1995; Laurance, 1991; Laurance and Yensen, 1991; Kapos et al., 1993; Lovejoy et al., 1986; Reed et al., 1996; Wilcove et al., 1986).

Many types of ecosystem edge effect dynamics have been identified, including changes in the rate of leaf litter decomposition (Didham, 1998), changes in soil moisture, abrupt changes in wind speed (Ranny et al., 1981), changes in light penetration and solar radiation (Ranny et al., 1981), and changes in nutrient hydrological cycling (Saunders et al., 1990).

Despite different types of ecosystem representation, edge effects are most common in moderately to highly fragmented landscapes (Donovan et al., 1997; Hartley and Hunter, 1998; Thompson et al., 2002) and are less pronounced in large fragments where there is a lower perimeter-area ratio (Helzer and Jelinski, 1999). Edge effects are greatest where relatively small but different areas are juxtaposed (Keyser et al., 1998; Storch et al., 2005).

Although ecological edges are often recognized as borders between human-disturbed and natural landscapes (Ewers and Didham, 2006; Lindenmayer and Fischer, 2006; Murcia, 1995), but they also occur where natural ecosystem transitions occur (Young et al., 2012), so they may have conceptual applicability both in karst to non-karst transitions and within karst areas.

Karst in the Guilin area is a mixture of tower and cockpit karst styles, with transitions between them (Zhu et al., 1988). Two groups of hypotheses present opposing views regarding the evolution of tropical karst. Sequential models based upon Davis's theory of a Geographical Cycle (1899) have regarded tower karst and cockpit karst as different stages of landscape evolution (Sweeting, 1958, 1990; Gerstehauer, 1960; Song et al., 1983; Williams, 1985; He, 1986), suggesting that tower karst has evolved from cockpit karst, and that thus the former is an "older" stage of the latter. By contrast, parallel models have proposed that tower karst and cockpit karst have evolved simultaneously without distinctive erosional stages (Verstappen, 1960, Balazs, 1968; Yuan 1981, 1986; Williams, 1986; Yuan et al., 1990; Tan 1992; Sweeting, 1995 and Zhu et al., 1988). Employing the ecological analogy, it is highly possible that there is an edge effect in tropical karst where tower karst and cockpit coexist, particularly if the former represents the edge effect or transition between karst and non-karst (Day and Huang, 2009). It is

hypothesized that tower karst necessarily occurs peripheral to or integrated with larger, contiguous areas of cockpit karst, while the existence of cockpit karst does not necessarily require the existence of tower in its proximity.

Geomorphological edge effects may both parallel and differ from biological edges in terms of morphologies and processes. Initially, in this study the potential edge effects are examined in terms of the geographic positioning of tower and cockpit karst landscapes, with secondary attention to process variations. By contrast and comparison, biological edge effects are concerned with the distribution, abundance and persistence of species, or with biological process variations (Ewers and Didham, 2006; Lindenmayer and Fischer, 2006; Murcia, 1995; Ries and Sisk, 2004).

This is the first study to try to identify the existence of edge effects in tropical karst, and there has been no real consideration of how geomorphological/environmental variables contribute to the formation of the edge. Defining the concept and testing the basic hypothesis are thus of fundamental importance, and may ultimately help to explain the evolution of tropical karst. This study of potential edge effects involving tower karst and cockpit karst in the Guilin area is thus the first to define and attempt to identify this phenomenon in tropical karst landscapes.

In order to examine the potential edge effects, this study will test the following hypotheses: (1) Cockpit karst may develop independently on its own, and is not necessarily associated with tower karst. (2) The development of tower karst requires association with cockpit karst. (3) The coexistence of tower and cockpit landforms in a given area reflects the similarity of their development conditions, but the two landforms are the results of differing intensity of influential factors, such as NDVI, bicarbonate

concentrations, and surface drainage, exerted across the same open system over heterogeneous temporal and spatial scales.

5.2 Study area and data

The study was conducted in Guilin, Guangxi, China, where there is a pronounced mixture of tower karst and cockpit karst. The geographic location of tower karst and cockpit karst are based on the classification results from chapter 2, corrected NDVIs are based on the topographic correction and shadow restoration from chapter 3, and hydrological control factors (bicarbonate ions) are from chapter 4.

5.3 Methodology

The nearest neighbor distances between tower karst (100 samples), cockpit karst (100 samples) and stream networks were calculated by using the proximity tools available via the analysis tools in ArcGIS.

Geographic locations of tower karst (TK) and cockpit karst (CK) in both horizontal (longitude) and vertical direction (latitude) were set as dependent variables, while the nearest neighbor distance between tower karst, cockpit karst and stream networks, corrected NDVI after topographic correction and shadow restoration, precipitation, and the hydrological control factors (bicarbonate ions) were set as independent variables. One hundred samples of fenglin and one hundred samples of fengcong were prepared for the analysis, respectively. The data sets were introduced to IBM SPSS V22.0 software to

conduct a stepwise regression analysis. Prior to the regression analysis, correlation between the independent variables was also checked.

After the stepwise regression analysis, the spatial autocorrelation analysis for fenglin and fengcon in horizontal and vertical directions was obtained through the global Moran's I calculation.

5.4 Results and discussions

5.4.1 Stepwise regression results for fenglin (TK)

Tables 4 through 6 display the correlation between fenglin locations (TK_LAT) and the influential factors in the vertical direction. NDVI, bicarbonate (BICAR), rainfall and distant to fengcong (DIST2CK) have positive correlations with the vertical location of fenglin. Results of stepwise regression (Table 5 and 6) show that the vertical distributions of fenglin are determined by both distance to stream network and rainfall with an R square of 0.807.

Tables 7 through 9 display the correlation between fenglin locations (TK_LON) and the influential factors in the horizontal direction. Differing from the vertical direction result, only bicarbonate (BICAR) has a positive correlation with the horizontal location of fenglin, with other factors showing negative correlations. Results of stepwise regression (Tables 8 and 9) show that the horizontal distribution of fenglin is determined by distance to stream network, rainfall and concentration of bicarbonate, with an R square of 0.967.

Table 4. Correlation between tower karst latitude and other variables

		Correlations					
		LAT	NDVI	BICAR	Rainfall	DIST2CK	DIST2HYDRO
Pearson Correlation	LAT	1.000	.427	-.398	.500	.077	-.628
	NDVI	.427	1.000	-.094	.658	.327	.082
	BICAR	.398	-.094	1.000	-.142	-.418	-.581
	Rainfall	.500	.658	-.142	1.000	.203	.205
	DIST2CK	.077	.327	-.418	.203	1.000	-.042
	DIST2HYDRO	-.628	.082	-.581	.205	-.042	1.000
Sig. (1-tailed)	LAT	.	.015	.022	.005	.355	.000
	NDVI	.015	.	.324	.000	.052	.345
	BICAR	.022	.324	.	.245	.017	.001
	Rainfall	.005	.000	.245	.	.160	.158
	DIST2CK	.355	.052	.017	.160	.	.419
	DIST2HYDRO	.000	.345	.001	.158	.419	.

Table 5. Model summary between tower karst latitude and other variables

Model Summary ^c									
Model	R	R Square	Adjusted R Square	Std. Error of the Estimate	Change Statistics				
					R Square Change	F Change	df1	df2	Sig. F Change
1	.628 ^a	.394	.369	.0003604	.394	15.629	1	98	.001
2	.898 ^b	.807	.790	.0002078	.413	49.197	1	97	.000

a. Predictors: (Constant), DIST2HYDRO

b. Predictors: (Constant), DIST2HYDRO, Rainfall

c. Dependent Variable: TK_LAT

□

Table 6. Model coefficients between tower karst latitude and other variables

Coefficients ^a											
Model		Unstandardized Coefficients		Standardized Coefficients	t	Sig.	Correlations			Collinearity Statistics	
		B	Std. Error	Beta			Zero-order	Partial	Part	Tolerance	VIF
1	(Constant)	.251	.000		2126.792	.000					
	DIST2HYDRO	-.002	.000	-.628	-3.953	.001	-.628	-.628	-.628	1.000	1.000
2	(Constant)	.224	.004		58.632	.000					
	DIST2HYDRO	-.002	.000	-.762	-8.149	.000	-.628	-.862	-.746	.958	1.044
	Rainfall	.161	.023	.656	7.014	.000	.500	.825	.642	.958	1.044

a. Dependent Variable: TK_LAT

□

Table 7. Correlation between tower karst longitude and other variables

		Correlations					
		LON	NDVI	BICAR	Rainfall	DIST2CK	DIST2HYDRO
Pearson Correlation	LON	1.000	-.498	0.546	-.737	-.105	-.776
	NDVI	-.498	1.000	-.094	.658	.327	.082
	BICAR	.546	-.094	1.000	-.142	-.418	-.581
	Rainfall	-.737	.658	-.142	1.000	.203	.205
	DIST2CK	-.105	.327	-.418	.203	1.000	-.042
	DIST2HYDRO	-.776	.082	-.581	.205	-.042	1.000
Sig. (1-tailed)	LON	.	.002	.005	.000	.304	.000
	NDVI	.002	.	.324	.000	.052	.345
	BICAR	.005	.324	.	.245	.017	.001
	Rainfall	.000	.000	.245	.	.160	.158
	DIST2CK	.304	.052	.017	.160	.	.419
	DIST2HYDRO	.000	.345	.001	.158	.419	.

Table 8. Model summary between Tower karst longitude and other variables

Model Summary ^d									
Model	R	R Square	Adjusted R Square	Std. Error of the Estimate	Change Statistics				
					R Square Change	F Change	df1	df2	Sig. F Change
1	.776 ^a	.603	.586	.0000094	.603	36.414	1	98	.000
2	.975 ^b	.951	.947	.0000034	.348	163.960	1	97	.000
3	.983 ^c	.967	.963	.0000028	.016	10.738	1	96	.003

a. Predictors: (Constant), DIST2HYDRO

b. Predictors: (Constant), DIST2HYDRO, Rainfall

c. Predictors: (Constant), DIST2HYDRO, Rainfall, BICAR

d. Dependent Variable: TK_LON

Table 9. Model coefficients between tower karst longitude and other variables

Model		Coefficients ^a										
		Unstandardized Coefficients		Standardized Coefficients	t	Sig.	Correlations			Collinearity Statistics		
		B	Std. Error	Beta			Zero-order	Partial	Part	Tolerance	VIF	
1	(Constant)	.110	.000		35702.543	.000						
	DIST2HYDRO	-6.476E-5	.000	-.776	-6.034	.000	-.776	-.776	-.776	1.000	1.000	
2	(Constant)	.111	.000		1786.140	.000						
	DIST2HYDRO	-5.445E-5	.000	-.653	-13.861	.000	-.776	-.945	-.639	.958	1.044	
	Rainfall	-.005	.000	-.603	-12.805	.000	-.737	-.936	-.590	.958	1.044	
3	(Constant)	.111	.000		1608.605	.000						
	DIST2HYDRO	-5.523E-5	.000	-.662	-16.729	.000	-.776	-.963	-.646	.953	1.049	
	Rainfall	-.004	.000	-.490	-9.354	.000	-.737	-.894	-.361	.544	1.839	
	BICAR	-1.399E-5	.000	-.169	-3.277	.003	-.546	-.573	-.127	.564	1.774	

a. Dependent Variable: TK_LON

5.4.2 Stepwise regression results for fengcong (CK)

Tables 10 through 12 display the correlation between fengcong locations (CK_LAT) and the influential factors in the vertical direction. NDVI, bicarbonate (BICAR) and rainfall have positive correlations with the horizontal location of fengcong, with distance to fenglin (DIST2TK) and distance to surface stream (DIST2HYDRO) showing negative correlations. Results of stepwise regression (Tables 11 and 12) show that the vertical distributions of fengcong are determined by bicarbonate, distance to stream network and rainfall, with an R square of 0.970. It is negatively correlated with the distance to near stream network (DIST2HYDRO), which suggests that the proximity of surface water does not favor the development of fengcong in the vertical direction.

Tables 13 through 15 display the correlations between fengcong locations (CK_LON) and the influential factors in the horizontal direction. Only the distance to fenglin (DIST2TK) shows a positive correlation with the horizontal location of fengcong, with NDVI, bicarbonate (BICAR), rainfall and distance to near surface stream (DIST2HYDRO) showing negative correlations. Results of stepwise regression (Tables

14 and 15) show that the horizontal distributions of fengcong are determined by rainfall and distance to stream network, with an R square of 0.922.

Table 10. Correlation between cockpit karst latitude and other variables

		Correlations					
		LAT	NDVI	BICAR	Rainfall	DIST2TK	DIST2HYDRO
Pearson Correlation	LAT	1.000	.118	.959	.547	-.487	-.365
	NDVI	.118	1.000	.068	.120	.179	-.103
	BICAR	.959	.068	1.000	.493	-.476	-.292
	Rainfall	.547	.120	.493	1.000	-.217	.437
	DIST2TK	-.487	.179	-.476	-.217	1.000	.094
	DIST2HYDRO	-.365	-.103	-.292	.437	.094	1.000
Sig. (1-tailed)	LAT	.	.184	.000	.000	.000	.002
	NDVI	.184	.	.304	.180	.085	.217
	BICAR	.000	.304	.	.000	.000	.012
	Rainfall	.000	.180	.000	.	.048	.000
	DIST2TK	.000	.085	.000	.048	.	.237
	DIST2HYDRO	.002	.217	.012	.000	.237	.

Table 11. Model summary between cockpit karst latitude and other variables

Model Summary ^d									
Model	R	R Square	Adjusted R Square	Std. Error of the Estimate	Change Statistics				
					R Square Change	F Change	df1	df2	Sig. F Change
1	.959 ^a	.920	.918	.0001386	.920	662.952	1	98	.000
2	.963 ^b	.927	.925	.0001327	.008	6.237	1	97	.015
3	.985 ^c	.970	.969	.0000858	.043	80.220	1	96	.000

a. Predictors: (Constant), BICAR

b. Predictors: (Constant), BICAR, DIST2HYDRO

c. Predictors: (Constant), BICAR, DIST2HYDRO, Rainfall

d. Dependent Variable: CK_LAT

Table 12. Model coefficient between cockpit karst latitude and other variables

Model		Coefficients ^a										
		Unstandardized Coefficients		Standardized Coefficients	t	Sig.	Correlations			Collinearity Statistics		
		B	Std. Error	Beta			Zero-order	Partial	Part	Tolerance	VIF	
1	(Constant)	.243	.000		906.322	.000						
	BICAR	.028	.001	.959	25.748	.000	.959	.959	.959	1.000	1.000	
2	(Constant)	.244	.000		880.019	.000						
	BICAR	.028	.001	.932	24.984	.000	.959	.957	.891	.915	1.093	
	DIST2HYDRO	.000	.000	-.093	-2.497	.015	-.365	-.314	-.089	.915	1.093	
3	(Constant)	.234	.001		209.996	.000						
	BICAR	.021	.001	.707	20.314	.000	.959	.938	.469	.439	2.276	
	DIST2HYDRO	-.001	.000	-.303	-9.013	.000	-.365	-.769	-.208	.470	2.129	
	Rainfall	.070	.008	.331	8.957	.000	.547	.767	.207	.389	2.572	

a. Dependent Variable: CK_LAT

Table 13. Correlation between cockpit karst longitude and other variables

		Correlations					
		LON	NDVI	BICAR	Rainfall	DIST2TK	DIST2HYDRO
Pearson Correlation	LON	1.000	-.009	-.248	-.852	.287	-.771
	NDVI	-.009	1.000	.068	.120	.179	-.103
	BICAR	-.248	.068	1.000	.493	-.476	-.292
	Rainfall	-.852	.120	.493	1.000	-.217	.437
	DIST2TK	.287	.179	-.476	-.217	1.000	.094
	DIST2HYDRO	-.771	-.103	-.292	.437	.094	1.000
Sig. (1-tailed)	LON	.	.474	.028	.000	.013	.000
	NDVI	.474	.	.304	.180	.085	.217
	BICAR	.028	.304	.	.000	.000	.012
	Rainfall	.000	.180	.000	.	.048	.000
	DIST2TK	.013	.085	.000	.048	.	.237
	DIST2HYDRO	.000	.217	.012	.000	.237	.

Table 14. Model summary between cockpit karst longitude and other variables

		Model Summary ^c							
Model	R	R Square	Adjusted R Square	Std. Error of the Estimate	Change Statistics				
					R Square Change	F Change	df1	df2	Sig. F Change
1	.852 ^a	.725	.721	.0000110	.725	153.124	1	98	.000
2	.960 ^b	.922	.920	.0000059	.197	144.649	1	97	.000

a. Predictors: (Constant), Rainfall

b. Predictors: (Constant), Rainfall, DIST2HYDRO

c. Dependent Variable: CK_LON

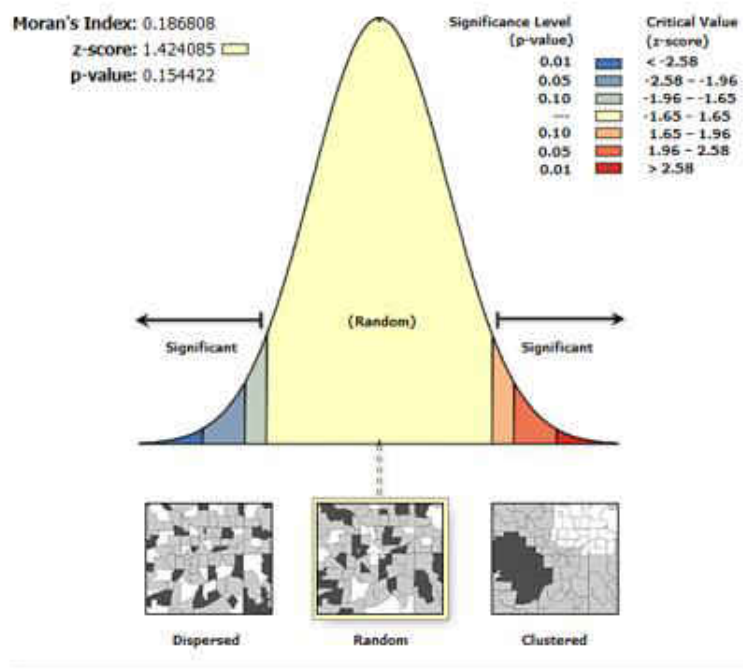
Table 15. Model coefficients between cockpit karst longitude and other variables

Model		Coefficients ^a										
		Unstandardized Coefficients		Standardized Coefficients	t	Sig.	Correlations			Collinearity Statistics		
		B	Std. Error	Beta			Zero-order	Partial	Part	Tolerance	VIF	
1	(Constant)	.112	.000		1081.711	.000						
	Rainfall	-.008	.001	-.852	-12.374	.000	-.852	-.852	-.852	1.000	1.000	
2	(Constant)	.111	.000		1824.132	.000						
	Rainfall	-.006	.000	-.636	-15.509	.000	-.852	-.899	-.572	.809	1.235	
	DIST2HYDRO	-5.476E-5	.000	-.493	-12.027	.000	-.771	-.847	-.444	.809	1.235	

a. Dependent Variable: CK_LON

5.4.3 Spatial autocorrelation results for fenglin (TK)

The global Moran's I for fenglin in the vertical direction (Figure 29) and horizontal direction (Figure 30) show similar values of Moran's index at around 0.186, suggesting that they are somewhat random in overall spatial distribution across the study area.



Given the z-score of 1.42, the pattern does not appear to be significantly different than random.

Figure 29. Global Moran's I for Fenglin in vertical direction

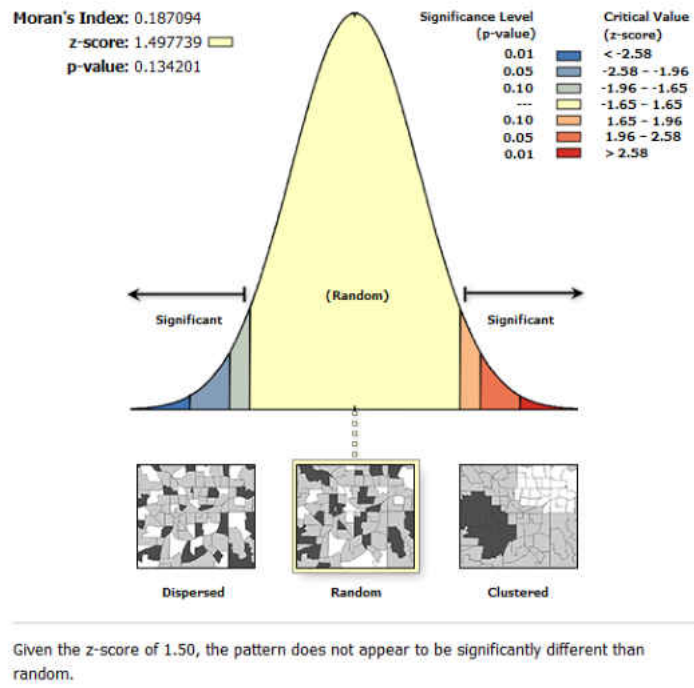
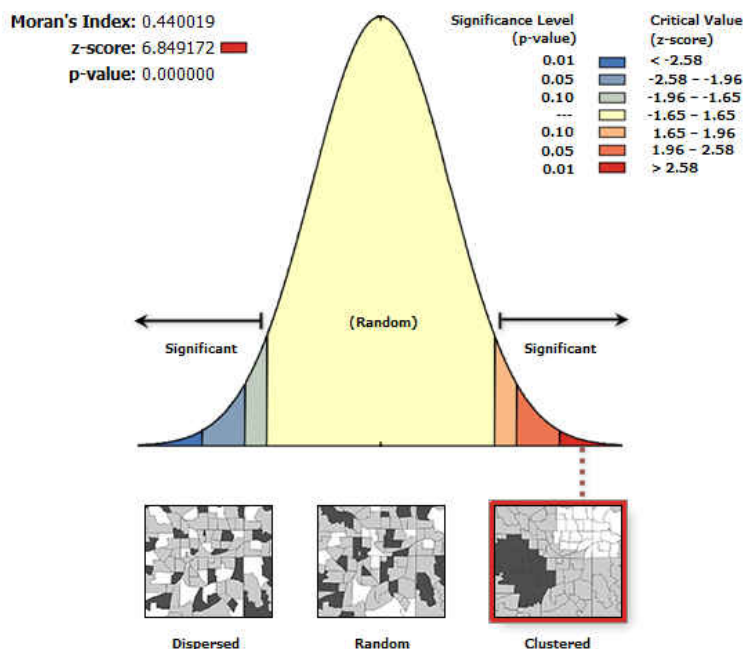


Figure 30. Global Moran's I for Fenglin in horizontal direction

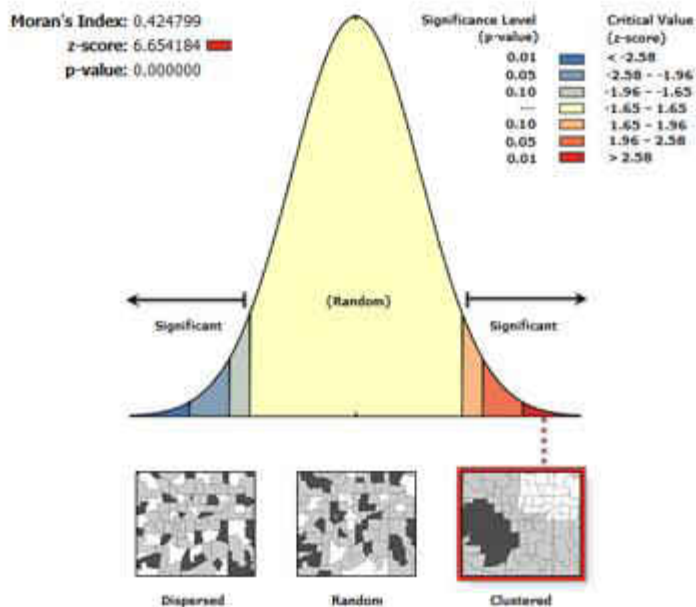
5.4.4 Spatial autocorrelation results for fengcong (CK)

The global Moran's I for fengcong in the vertical direction (Figure 31) and horizontal direction (Figure 32) show similar values of Moran's index around 0.4 and a z-score more than 0.6, suggesting that they are clustered pattern in overall spatial distribution across the study area.



Given the z-score of 6.85, there is a less than 1% likelihood that this clustered pattern could be the result of random chance.

Figure 31. Global Moran's I for Fengcong in vertical direction



Given the z-score of 6.65, there is a less than 1% likelihood that this clustered pattern could be the result of random chance.

Figure 32. Global Moran's I for Fengcong in horizontal direction

The first hypothesis is thus supported by the regression analysis result (Tables 10 to 15), because the distribution of fengcong is not strongly associated with the fenglin in both (Distance to fenglin or DIST2TK) in both vertical and horizontal direction. In addition, fengcong distribution is correlated with both rainfall (autogenic input) and distance to hydro, suggesting that it can develop independently, and does not necessarily require an association with fenglin.

Concerning the second hypothesis, the study supports the hypothesis that the development of fenglin does require an association with fengcong, particularly in the horizontal direction. This is because the bicarbonate (allogenic input) is generally injected in the bordering fengcong area, then it will pass through the groundwater network and discharge from the outlet or spring in the fenglin area (Ford and Williams, 1989).

The study also supports the third hypothesis. The regression analysis and spatial autocorrelation analysis, show that fenglin and fengcong may coexist in the same area, but that their respective development is associated with variable intensities of different input factors, such as NDVI, bicarbonate concentrations, rainfall and surface drainage. The vegetation factor (NDVI) is not a determining factor in either fenglin or fengcong distribution probably because it is outweighed by hydrological factors and bicarbonate distributions.

5.5 Conclusion

The study investigates the edge effects in tropical karst areas using a case study of Guilin in a fragmented tower-cockpit karst landscape. The results show that the edge effect does exist in the Guilin area, with variable intensities in different directions (vertical and

horizontal). In addition, the study also demonstrates that the fenglin distribution exhibits a random pattern while the fengcong is more clustered in the study area.

CHAPTER 6 CONCLUSIONS

6.1 Summary

Tower karst (fenglin) and cockpit karst (fengcong) are two important representative styles in tropical karst regions. Previous studies proposed sequential and parallel models of evolution, but they provide insufficient evidence to illuminate the spatial and temporal relationships between the two landforms. This unclear interpretation of tower-cockpit relationships both obscures understanding of the process-form dynamics, and also confuses the morphological definitions. Prior technological limitations, as well as the fragmental nature of the karst landscape, limited incorporation of geologic and hydrologic data into broad geospatial frameworks using GIS and RS techniques, and most of this data is scattered. Postulated edge effects have not previously been investigated, and little is known about how different environmental variables (geomorphology, vegetation, hydrological control, precipitation) contribute to the dynamics and morphology edges. To address these issues, this research has combined geographic, geologic and hydrologic data using GIS and RS technologies to generate solid and reliable quantitative evidence of the edge effect. Specifically, there were four purposes of the study. The first was to develop an effective method of differentiating fenglin and fengcong. The second was to extract the vegetation information without ignoring the shadows on the satellite imagery, and investigate the correlation between the karst topography and its vegetation. The third was to combine the regional hydrology and solute transport models to estimate geochemical controls over fenglin and fengcong. The

fourth, perhaps the most important objective, was to test the edge effect hypothesis using the results from the aforementioned three components.

The results of the dissertation lead to several significant conclusions. First, DEM data are very useful for extracting profiles of complicated surface landforms with shadows on the satellite imagery. Second, the vegetation distribution varies within and between tower karst and cockpit karst, and such differences correlate with their topographic characteristics. The under-representation of vegetation in the south-southwest aspect of tower karst was remarkable, and its overall distribution is less abundant and dispersed than in cockpit karst. Third, testing supported the edge effect hypothesis, showing variable intensity and extension in different directions. Additionally, the study also shows that the fenglin is distributed in a random pattern, while the fengcong is clustered within the study area.

6.2 Contribution

The first contribution of this study is highlighted by developing a method to classify tropical karst effectively in the presence of shadows that would otherwise hinder traditional approaches from classifying the complicated landforms. Second, the study suggests non-random variance of vegetation vitality in certain aspects of fenglin that could explain its geomorphic difference from fengcong. Third, the study developed a method to combine the groundwater and solute transport models to estimate bicarbonate concentration distribution. Finally, for the first time, the study supported the edge effect hypothesis through a systematic and quantitative approach, which may lead to new insights via similar studies in the future.

6.3 Future research

Future research might usefully attempt to employ similar methodologies to other regions with similar climatic and geologic conditions that promote the development of the tower and cockpit styles of tropical karst. Central America (Belize, Guatemala), the Caribbean (Jamaica, Puerto Rico, Hispaniola and Cuba) and Southeastern Asia (Indonesia, Malaysia, Vietnam) constitute appropriate study areas where comparable results might be produced through similar analysis. It would be particularly valuable to ascertain whether the demonstrated cockpit-tower edge effect is universal or is constrained within certain geographic locations.

REFERENCES

- Andrén, H., 1995. Effects of landscape composition on predation rates at habitat edges. *Mosaic landscapes and ecological processes*, ed. Hansson, L., Fahrig, L., and Merriam, G. Springer Netherlands, Chapman and Hall, London, pp 225-255
- Asner, G.P., & Heidebrecht, K.B., 2003. Imaging spectroscopy for desertification studies: comparing AVIRIS and EO-1 Hyperion in Argentina drylands. *IEEE Transactions on Geoscience and Remote Sensing*, 41, 1283-1296.
- Asner, G.P., Knapp, D.E., Cooper, A.N., Bustamante, M.M.C., Olander, L.P., & Heidebrecht, K.B., 2005. Ecosystem structure throughout the Brazilian amazon from Landsat observations and automated spectral unmixing, *Earth Interactions*, 9 (1)
- Balazs, D., 1973. Relief types of tropical karst areas. Proceedings of the Symposium on Karst Morphogenesis. *Proceedings of International Geographical Union Regional Conference (Hungary)*, 16–32.
- Bolch, T., Kamp, U., Olsenholler, J., 2005. Using ASTER and SRTM DEMs for studying geomorphology and glaciation in high mountain areas. *New Strategies for European Remote Sensing*, ed. Oluic, M. Rotterdam: Millpress, 119–128.
- Bonacci, O., 1982. Specific hydrometry of karst regions. *Advances in Hydrometry*, IAHS Publ. 134, 321-333.
- Bonacci, O., 1995. Ground water behaviour in karst: example of the Ombla Spring (Croatia). *Journal of Hydrology*, 165(1), 113-134.

- Brook, G.A. and Hanson, M., 1991, Double Fourier series analysis of cockpit and doline karst near Browns Town, Jamaica. *Physical Geography*, 12(1), 37-54
- Bubenzer, O. and Bolten, A., 2008. The use of new elevation data (SRTM/ASTER) for the detection and morphometric quantification of Pleistocene megadunes (draa) in the eastern Sahara and the southern Namib. *Geomorphology*, 102, 221–231.
- Chen, Y., Wen, D., Jing, L., and Shi, P., 2007. Shadow information recovery in urban areas from very high resolution satellite imagery. *International Journal of Remote Sensing*, 28(15): 3249-3254.
- Chenoweth, M.S. and Day, M.J., 2001. Developing a GIS for the Jamaican Cockpit Country. *Geotechnical and environmental applications of karst geology and hydrology*, ed. Beck B.F. and Herring J.G. Swets & Zeitlinger Publishers, Lisse, Netherlands, 67–71
- Dare, P.M., 2005. Shadow analysis in high-resolution satellite imagery of urban areas. *Photogrammetric Engineering and Remote Sensing*, 71,169–177
- Day, M. J., 1978. Morphology and distribution of residual limestone hill in the karst of northern Puerto Rico. *Geological Society of America Bulletin*, 89(3), 426-432
- Day, M.J. 1979. Surface roughness as a discriminator of tropical karst styles. *Zeitschrift fur Geomorphologie, Supplementbande*, 32, 1-8.
- Day, M.J., 1981. Towards numerical categorization of tropical karst terrains. *Proceedings of 8th International Congress of Speleology*, 1, 330-332.
- Day, M. J., 1982. The influence of some material properties on the development of tropical karst terrains. *Transactions of British Cave Research Association*, 9 (1), 27-37

- Day, M.J., 2002. The role of valley systems in the evolution of tropical karstlands. In: *Evolution of Karst: From Prekarst to Cessation*, ed. F. Gabrovsek. Založba ZRC, Ljubljana, 235-241.
- Day, M.J., 2004a. Cone karst, in *Encyclopedia of Caves and Karst Science*, ed. Gunn, J. New York: Fitzroy Dearborn, 241-243.
- Day, M. J., 2004b. Morphometry of Karst, in *Encyclopedia of Caves and Karst Science*, ed. Gunn, J. New York: Fitzroy Dearborn, 526-527.
- Day, M.J. and Chenoweth, M.S., 2004. The Karstlands of Trinidad and Tobago, their land use and conservation. *The Geographical Journal*, 170 (3), 256-266.
- Day, M.J. and Chenoweth, M.S., 2013a. Cockpit Country Cone Karst, Jamaica, *Encyclopedia of Caves and Karst Science*, ed. Gunn, J. New York: Fitzroy Dearborn, 233-235.
- Day, M.J. and Chenoweth, M.S., 2013b. Surface roughness of karst landscapes, *Treatise on Geomorphology*, Volume 6, Karst Geomorphology, ed. Frumkin, A, New York: Academic Press: 157-163.
- Day, M.J. and Tang, T., 2004. Tower karst. *Encyclopedia of Caves and Karst Science*, ed. Gunn, J. New York: Fitzroy Dearborn, 734-736.
- Day, M.J. and Huang, W., 2009. Reflections on fengcong and fenglin. *Cave and Karst Science*, 36(2), 49-51.
- Didham, R.K., 1998. Altered leaf-litter decomposition rates in tropical forest fragments. *Oecologia*, 116(3), 397-406.
- Donovan, T.M., Jones, P.W., Annand, E.M., and Thompson III, F.R., 1997. Variation in

local-scale edge effects: mechanisms and landscape context. *Ecology*, 78(7), 2064–2075.

Doummar, J., Sauter, M., and Geyer, T., 2012. Simulation of flow processes in a large scale karst system with an integrated catchment model (Mike She)–Identification of relevant parameters influencing spring discharge. *Journal of Hydrology*, 426, 112-123.

Ewers, R.M., and Didham, R.K., 2006. Confounding factors in the detection of species responses to habitat fragmentation. *Biological Reviews*, 81(1), 117–142.

Faulkner, J., Hu, B. X., Kish, S., and Hua, F., 2009. Laboratory analog and numerical study of groundwater flow and solute transport in a karst aquifer with conduit and matrix domains. *Journal of contaminant hydrology*, 110(1), 34-44.

Field, M.S., 1997. Risk assessment methodology for karst aquifers:(2) solute-transport modeling. *Environmental Monitoring and Assessment*, 47(1), 23-37.

Fleurant, C., Tucker, G.E. and Viles, H.A. 2007. Modele d'évolution de paysages, application au karstes en cockpit de Jamaïque. *Karstologia*, 49: 33-42.

Fleurant, C., Tucker, G.E. and Viles, H.A. 2008a. Modelling cockpit karst landforms. in: *Landscape Evolution: Denudation, Climate and Tectonics over Different Time and Space Scales*, ed. Gallagher, K., Jones, S.J. and Wainwright, J. London: Geological Society Special Publication 296: 47-62

Fleurant, C., Tucker, G.E. and Viles, H.A. 2008b. A model of cockpit karst landscape, Jamaica. *Géomorphologie: relief, processus, environnement*, 1, 3-14.
<http://geomorphologie.reviews.org/index5653.html>

- Fleury, P., Plagnes, V., and Bakalowicz, M., 2007. Modelling of the functioning of karst aquifers with a reservoir model: Application to Fontaine de Vaucluse (South of France). *Journal of hydrology*, 345(1), 38-49.
- Ford, D. C., Palmer, A. N., and White, W. B., 1988. Landform development; karst. Geological Society of America. 2, 401-412
- Ford, D.C., and Williams, P.W., 1989. *Karst geomorphology and hydrology*. London: Unwin Hyman, 601pp
- Ford, D.C. and Williams, P.W., 2007. *Karst Hydrogeology and Geomorphology*, Chichester; Wiley, 562pp.
- Gao, Y., Zhang, W., 2009. LULC classification and Topographic Correction of Landsat-7 ETM + Imagery in the Yangjia RivernWatershed: The influence of DEM Resolution Sensors. *Sensor*, 9(3): 1980–1995.
- Gellert, J.F. 1962. Der Tropenkarst in Sub-china im Rahmen der Gebirgsformung des landes. *Verhandlungen des Deutschen Geographentages*, 33, 376-84.
- Giles, P.T., 2001. Remote sensing and cast shadows in mountainous terrain. *Journal of the American Society for Photogrammetry and Remote Sensing*, 67(7), 833-839
- Goldscheider, N., and Ravbar, N. 2007. Proposed methodology of vulnerability and contamination risk mapping for the protection of karst aquifers in Slovenia. *Acta carsologica*, 36(3), 397-411
- Guilin Karst and Geological Structure, 1988, Chongqing Pressing House, 130 pp

Guo, L., and Chen, Z., 2006. The Puzzles and Solutions for Quantitative Assessment of Water Resource in Karst Underground River System. *Carsologica Sinica*, 25(1), 1-5 (in Chinese)

Haboudane, D., Miller, J.R. and Pattey, E., 2004. Hyperspectral Vegetation Indices and Novel Algorithms for Predicting Green LAI of Crop Canopies: Modeling and Validation in the Context of Precision Agriculture. *Remote Sensing of Environment*, 90: 337–352.

Harbaugh, A. W., 2005. *MODFLOW-2005, the US Geological Survey modular ground-water model: The ground-water flow process* (pp. 6-A16). US Department of the Interior, US Geological Survey.

Harden, C.P., 2002. Hillslope runoff, soil detachment, and soil organic content following reforestation in the Copper Basin, Tennessee, USA. *Australian Geographical Studies* 40 (2), 130–142.

Hartley, M.J., and Hunter, M.L., 1998. A meta-analysis of forest cover, edge effects, and artificial nest predation rates. *Conservation Biology*, 12(2), 465–469.

Helzer, C.J., and Jelinski, D.E., 1999. The relative importance of patch area and perimeter area ratio to grassland breeding birds. *Ecological applications*, 9(4), 1448–1458.

Hodgson, M. E., Jensen, J. R., Tullis, J. A., Riordan, K. D., & Archer, C. M., 2003. Synergistic use of Lidar and color aerial photography for mapping urban parcel imperviousness. *Photogrammetric Engineering and Remote Sensing*, 69, 973–980.

- Huang, J., Yan, Q., Wang, M., Zhou, W., Gua, C., Shi, J., Pei, J., Huang, J. and Li, Q., 1988. Study on karst water resource evaluations in *Guilin and its methodology*. Chongqing Publishing House. 134 pp. (in Chinese)
- Huang, W., Deng, C., and Day, M.J., 2014. Differentiating tower karst (fenglin) and cockpit karst (fengcong) using DEM contour, slope, and centroid. *Environmental Earth Sciences*. 72(2): 407-416
- Huang, Z., Turner, B. J., Dury, S. J., Wallis, I. R., & Foley, W. J. 2004. Estimating foliage nitrogen concentration from HYMAP data using continuum removal analysis. *Remote Sensing of Environment*, 93(1), 18-29.
- Hutchinson, M.F. and Gallant, J.C., 2000. Digital elevation model and representation of terrain shape. *Terrain Analysis: Principle and Application*, ed. Gallant, J.C and Wilson, J.P. New York: Wiley: 29-50.
- Jakucs, L., 1977. *Morphogenetics of karst regions: Variants of karst evolution*. Budapest: Akademiai Kiado, p284
- Jeannin, P.Y., and Sauter, M., 1998. Analysis of karst hydrodynamic behaviour using global approaches: a review. *Bulletin Centre d'Hydrogéologie*, Université de Neuchatel, 16, 31-48.
- Jensen, J., 2007. *Introductory Digital Image Processing*. Beijing: Science Press and Pearson Education Asia Limited, China, 127–173, 220–221.
- Jones, A. R., Settle, J. J., and Wyatt, B. K., 1988. Use of digital terrain data in the interpretation of SPOT-1 HRV multispectral imagery. *Remote Sensing*, 9(4), 669-682.

- Kapos, V., Ganade, G., Matsui, E., and Victoria, R.L., 1993. Carbon 13 isotope as an indicator of edge effects in tropical rainforest reserves. *Journal of Ecology*, 81, 425-432.
- Keesstra, S.D., van Dam, O., Verstraeten, G., van Huissteden, J., 2009. Changing sediment dynamics due to natural reforestation in the Dragonja catchment, SW Slovenia. *Catena*, 78 (1), 60–71.
- Keyser, A. J., Hill, G. E., and Soehren, E.C., 1998. Effects of Forest Fragment Size, Nest Density, and Proximity to Edge on the Risk of Predation to Ground - Nesting Passerine Birds. *Conservation Biology*, 12(5), 986-994.
- Kim, M.K., and Daigle, J.J., 2011. Detecting Vegetation Cover Change on the Summit of Cadillac Mountain Using Multi-Temporal Remote Sensing Datasets: 1979, 2001, and 2007. *Environmental Monitoring and Assessment*, 180, 63–75.
- Kincaid, T., 2004. Exploring the secrets of Wakulla Springs. In *open seminar, Tallahassee*.
- Kohavi, R and Provost, F., 1998. Glossary of Terms. In: Editorial for the Special Issue on Applications of Machine Learning and the Knowledge Discovery Process, *Machine Learning*, 30, 271-274
- Kokaly, R. F., 2001. Investigating a physical basis for spectroscopic estimates of leaf nitrogen concentration. *Remote Sensing of Environment*, 75, 153-161.
- Laurance, W.F. 1991. Edge effects in tropical forest fragments: application of a model for the design of nature reserves. *Biological Conservation*, 57(2), 205-219.
- Laurance, W.F. and Yensen, E., 1991. Predicting the impacts of edge effects in fragmented habitats. *Biological Conservation*, 55(1), 77-92.

LeGrand, H. E., and Stringfield, V. T., 1973. Karst hydrology—a review. *Journal of Hydrology*, 20(2), 97-120.

Liang, F and Xu, B., 2013. Discrimination of tower-, cockpit-, and non-karst landforms in Guilin, Southern China, based on morphometric characteristics, *Geomorphology*, 204, 42-48

Lindenmayer, D.B., and Fischer, J., 2006. *Habitat Fragmentation and Landscape Change: an Ecological and Conservation Synthesis*. Island Press, Washington, DC.

Liu, W., and Yamazaki, F., 2012. Object-based shadow extraction and correction of high-resolution optical satellite images. *IEEE Journal of Selected Topics in Applied Earth Observation and Remote Sensing*, 5(4), 1296–1302.

Liu, Z., 1991. IGCP 299 "Geology, Climate, Hydrology and Karst Formation" *Guidebook for Field Excursions of International Symposium and Field Seminar on Karst of Inner Plate Region with Monsoon Climate*. P1-18. The Institute of Karst Geology

Lovejoy, T.E., Bierregaard, Jr. R.O., Rylands, A.B., Malcolm, J.R., Quintela, C.E., Harper, L. H., Brown, K.S., Powell, A.H., Powell, G.V.N., Schubert, H.O.R., and Hays, M.B., 1986. Edge and other effects of isolation on Amazon forest fragments. *Conservation Biology: The Science and Scarcity of Diversity*, ed. Soule, M. Sunderland, Massachusetts, pp7-12

Lyw-Ayee, P. 2004. *Digital Topographic Analysis of Cockpit Karst: A Morphogeological Study of the Cockpit Country Region, Jamaica*, PhD thesis, University of Oxford.

- Lyew-Ayee, P., Viles, H.A. and Tucker, G.E. 2007. The use of GIS-based digital morphometric techniques in the study of cockpit karst. *Earth Surface Processes and Landforms*, 32(2), 165-179.
- Mangin, A., 1978. Le karst, entité physique, abordé par l'étude du système karstique. (Karst as a physical unit, from the study of the karst system) *Le karst, colloque de Tarbes*, 17-18
- Martínez-Santos, P., and Andreu, J. M., 2010. Lumped and distributed approaches to model natural recharge in semiarid karst aquifers. *Journal of hydrology*, 388(3), 389-398.
- Marston, R.A., Bravard, J.-P., Green, T., 2003. Impacts of reforestation and gravel mining on the Malnant River, Haute Savoie, French Alps. *Geomorphology* 55 (1–4), 65–74.
- Marston, R.A., 2010. Geomorphology and vegetation on hillslopes: Interactions, dependencies, and feedback loops. *Geomorphology*, 116, 206–217
- Mather, P.M., 2004. *Computer Processing of Remotely-Sensed Images*. London: John Wiley & Sons Ltd., 81 and 136.
- McDonald, M.G., and Harbaugh, A.W., 1988. A modular three-dimensional finite-difference groundwater flow model. *Techniques of water resources investigations*, 06-A 1. US Geophys Soc.
- McDonald, R.C. 1975. Observations on hillslope erosion in tower karst topography of Belize. *Geological Society of America Bulletin*, 86(2), 255–256.

McDonald, R.C. 1976a. Limestone morphology in South Sulawesi, Indonesia. *Zeitschrift für Geomorphologie, Supp*, 26, 79-91.

McDonald, R.C. 1976b. Hillslope base depressions in tower karst topography of Belize. *Zeitschrift für Geomorphologie, Supp*, 26, 98-103.

McDonald, R.C. 1979a. Tower karst geomorphology in Belize. *Zeitschrift für Geomorphologie Supp*, 32, 35-45

McDonald, R.C. 1979b. *Tower Karst Geomorphology, with Special Reference to Belize, Indonesia, and Malaysia*. Doctoral Dissertation, University of Oxford.

McDonald, R.C. 2002. Rivers in karst geomorphology, in *Evolution of Karst: From Prekarst to Cessation*, ed. Gabrovsek, F. Ljubljana: Zalozba SRC: 267-273

McDonald, R.C and Ley, R G. 1985. Tower karst geomorphology in northern Borneo. *Zeitschrift für Geomorphologie*, 29, 483–495.

McDonald, R.C and Twidale C.R., 2011, On the Origin and Significance of Basal Notches or Footcaves in Karst Terrains, *Physical Geography*, 32(3), 195-216

Miller, T., 1987. Fluvial and collapse influence on cockpit karst of Belize and eastern Guatemala. *Karst Hydrogeology: Engineering and Environmental Applications*, ed. B.F. Beck. Rotterdam: AA Balkema, 53-63

Murcia, C., 1995. Edge effects in fragmented forests: implications for conservation.

Trends in Ecology and Evolution, 10 (2), 58–62.

- Myloie, J.E. and Myloie, J.R., 2009. Caves as sea level and uplift indicators, Kangaroo Island, South Australia. *Journal of Cave and Karst Studies*, 71(1), 32-47.
- Nakajima, T., Tao, G., and Yasuoka, Y., 2002. Simulated recovery of information in shadow areas on IKONOS image by combining ALS data. *Proceedings of Asian Conference on Remote Sensing*. Retrieved at <http://www.gisdevelopment.com/aars/acrs/2002/vhr/214.pdf>.
- Palmer, A. N. 1975. The origin of maze caves. *National Speleological Society Bulletin*, 37(3), 56-76.
- Parise, M., J. D. Wales, and F. Gutierrez. 2009. Current Perspectives on the Environmental Impacts and Hazards in Karst. *Environmental Geology*, 58, 235–237.
- Purkis, S.J., Rowlands, G.P., Riegl, B.M., and Renaud, P.G., 2010, The paradox of tropical karst morphology in the coral reefs of the arid Middle East. *Geology*, 38, 227–230.
- Ranney, J.W., Bruner, M.C., and Levenson, J.B., 1981. The importance of edge in the structure and dynamics of forest islands. *Forest Island Dynamics in Man-Dominated Landscapes*, ed. Burgess a, R.L. and Sharpe, D.M. Springer Verlag, New York. pp 67-95
- Reed, R. A., Johnson-Barnard, J., and Baker, W.L., 1996. Fragmentation of a forested Rocky Mountain landscape, 1950–1993. *Biological Conservation*, 75(3), 267-277.
- Reinhardt, L., Jerolmack, D., Cardinale, B.J., Vanacker, V., Wright, J., 2010. Dynamic interactions of life and its landscape: feedbacks at the interface of geomorphology and ecology. *Earth Surface Processes and Landforms*, 35, 78–101.

- Renschler, C.S., Doyle, M.W., Thoms, M., 2007. Geomorphology and ecosystems: challenges and keys for success in bridging disciplines. *Geomorphology*, 89 (1–2),1–8.
- Riaño, D., Chuvieco, E., Salas, J., and Aguado, I., 2003. Assessment of different topographic corrections in Landsat-TM data for mapping vegetation types. *IEEE Transactions on Geoscience and Remote Sensing*, 41(5), 1056-1061.
- Ries, L., and Sisk, T.D., 2004. A predictive model of edge effects. *Ecology*, 85(11), 2917–2926.
- Roberts, D. A.; Smith, M. O.; Adams, J. B., 1993. Green Vegetation, Nonphotosynthetic Vegetation, and Soils in AVIRIS Data. *Remote Sensing of Environment*, 44 (2-3), 255-269
- Ru, J. et al.,1988. *The comprehensive study of Lijiang River Watershed Management*, Guangxi Normal University Publishing House, 59 pp (In Chinese)
- Salvador, E., Cavallaro, A and Ebrahimi,T., 2001. Shadow identification and classification using invariant color models. *Proceedings of IEEE International Conference of Acoustics Speech Signal Process.* vol.3, 1545–1548.
- Sarabandi, P., Yamazaki, F., Matsuoka, M., and Kiremidjian, A., 2004. Shadow detection and radiometric restoration in satellite high resolution images. *Proceedings of IGARSS-2004*, September 2004, Anchorage, Alaska (New York: IEEE), CDROM.
- Saunders, D.A., Hobbs, R.J., and Margules, C.R. 1990. Biological consequences of ecosystem fragmentation: a review. *Conservation Biology*, 5(1), 18-32.

- Scanlon, B.R., Mace, R.E., Barrett, M.E., and Smith, B., 2003. Can we simulate regional groundwater flow in a karst system using equivalent porous media models? Case study, Barton Springs Edwards aquifer, USA. *Journal of Hydrology*, 276(1), 137-158.
- Shackelford, A. K., and Davis, C. H., 2003. A hierarchical fuzzy classification approach for high-resolution multispectral data over urban areas. *IEEE Transactions on Geoscience and Remote Sensing*, 41(9), 1920-1932.
- Shahtahmassebi, A., Yang, N., Wang, K., Moore, N., and Shen, Z., 2013. Review of shadow detection and de-shadowing methods in remote sensing. *Chinese Geographical Science*, 23(4), 403-420.
- Šimůnek, J., and Suarez, D.L., 1994. Two dimensional transport model for variably saturated porous media with major ion chemistry. *Water Resources Research*, 30(4), 1115-1133.
- Smart, C.C., 1999. Subsidiary conduit systems: a hiatus in aquifer monitoring and modelling. *Proceedings of Karst modelling Symposium*, ed. Palmer, A.N., Palmer, M.V., and Sasowsky, I.D. Charlottesville, February 24–27, 1999. Karst Water Institute, Spec Publ 5, 146–157
- Smart, P., Waltham, T., Yang, M. and Zhang, Y., 1986. Karst geomorphology of western Guizhou, China. *Cave Science* 13: 89-103.
- Sweeting, M.M., 1972. *Karst Landforms*. London and New York: Macmillan, 362pp.
- Tang, T. and Day, M.J. 2000. Field survey and analysis of hillslopes on tower karst in Guilin, southern China. *Earth Surface Processes and Landforms*, 25: 1221-1235.

Teillet, P.M., Guindon, B., and Goodenough, D.G., 1982. On the slope-aspect correction of multispectral scanner data, *Canadian Journal of Remote Sensing*, 8(2), 84-106

Trimble, 2011. *eCognition Developer 8.64.1-User Guide*, Munchen: Trimble Germany GmbH., 242pp.

Trček, B., 2008. Flow and solute transport monitoring in the karst aquifer in SW Slovenia. *Environmental geology*, 55(2), 269-276.

Troester, J.W., 1992. The northern karst belt of Puerto Rico: A humid tropical karst, *Hydrogeology of selected karst regions of the world: International Association of Hydrogeologists, International Contributions to Hydrogeology*, 13, 475-486.

Tsai, V. J., 2006. A comparative study on shadow compensation of color aerial images in invariant color models. *IEEE Transactions on Geoscience and Remote Sensing*, 44(6), 1661-1671.

Tucker, C.J., 1979. Red and photographic infrared linear combinations for monitoring vegetation. *Remote Sensing of Environment*, 8, 127-150.

Waltham, T. 2008. Fengcong, fenglin, cone karst and tower karst. *Cave and Karst Science*, 35(3), 77-88.

Ustin, S.L., Roberts, D.A., Gamon, J.A., Asner, G.P., & Green, R.O., 2004. Using imaging spectroscopy to study ecosystem processes and properties. *Bioscience*, 54, 523-534.

Wang, S., Liu, Q., and Zhang, D., 2004. Karst Rocky Desertification in Southwestern China: Geomorphology, Landuse, Impact and Rehabilitation. *Land Degradation and Development*, 15, 115-121.

- Wang, S., and Li, Y., 2007. Problems and Development Trends about Researches on Karst Rocky Desertification. *Advance in Earth Sciences*, 6, 573–582.
- Waltham, T., 2008. Fengcong, fenglin, cone karst and tower karst. *Cave and Karst Science*, 35(3), 77–88.
- Weng, Q., 2012. Remote sensing of impervious surfaces in the urban areas: Requirements, methods, and trends. *Remote Sensing of Environment*, 117, 34–49
- White, W.B., 1988. *Geomorphology and hydrology of karst terrains*. New York: Oxford university press. pp 464
- White, W.B., 2002. Karst hydrology: recent developments and open questions. *Engineering geology*, 65(2), 85-105.
- Williams, P.W., 1972. Morphometric analysis of polygonal karst in New Guinea. *Geological Society of America Bulletin*, 83(3), 761-796.
- Williams, P.W., 1980, Hydrological control and the development of cockpit and tower karst, *Proceedings of IAH 21st Congress of Karst Hydrogeology and karst environment protection, Guilin, China*, 281-290
- Williams, P. W., 1985. Subcutaneous hydrology and the development of doline and cockpit karst. *Zeitschrift für Geomorphologie*, 29(4), 463-482.
- Williams, P.W., 1987. Geomorphic inheritance and the development of tower karst. *Earth Surface Processes and Landforms*, 12(5): 453-465.
- Yang, X., Skidmore, A. K., Melick, D., Zhou, Z., and Xu, J., 2007. Towards an efficacious method of using Landsat TM imagery to map forest in complex mountain terrain in Northwest Yunnan, China. *Tropical Ecology*, 48(2), 227.

- Yao, J. and Zhang, Z., 2006. Hierarchical shadow detection for color aerial images, *Computer Vision and Image Understanding*, 102, 60–69
- Yesilnacar, E., and Süzen, M.L., 2006. A land - cover classification for landslide susceptibility mapping by using feature components. *International Journal of Remote Sensing*, 27(2): 253-275.
- Yuan, D., 1984. *About Fengcong karst*. Geology of Guangxi 1, 79–84 (in Chinese).
- Yuan, D., 1985. On the heterogeneity of karst water. Karst water Resource. *Proceedings of the Ankara-Antalya Symposium*, IAHS Publ, 161, 281-292
- Yuan, D., 1991. *Karst of China*. Beijing: Geological Publishing House, 224pp.
- Yuan, D., 1992. Karst in Southwest China and its comparison with karst in north China. *Quaternary Sciences of China*. 4, 352-361 (in Chinese)
- Yuan D., 2004. Yangshuo karst, China, in *Encyclopedia of Caves and Karst Science*, ed. Gunn, J. Fitzroy Dearborn: New York, 781-783.
- Yuan, D., and Zhang, C., 2008. Karst Dynamics Theory in China and Its Practice. *Acta Geoscientica Sinica*, 29: 355–365.
- Yue, Y., Zhang, B., Wang, K., Liu, B., Li, R., Jiao, Q., Yang, Q., Zhang, M., 2010. Spectral indices for estimating ecological indicators of karst rocky desertification, *International Journal of Remote Sensing*, 31(8), 2115-2122.
- Yue, Y., Wang, K., Liu, B., Li, R., Zhang, B., Chen, H., and Zhang, M., 2013. Development of new remote sensing methods for mapping green vegetation and exposed

bedrock fractions within heterogeneous landscapes. *International Journal of Remote Sensing*, 34:14, 5136-5153.

Zeng, Z., 1982. Characters of the karst topography in southern China. *Carsologica Sinica* ,1, 27–31 (in Chinese).

Zhan, Q., Shi, W., and Xiao, Y., 2005. Quantitative analysis of shadow effects in high-resolution images of urban areas. *International Archives of Photogrammetry and Remote Sensing*, 36(8/W27). Available at: <http://www.isprs.org/proceedings/XXXVI/8-W27/zhan.pdf>

Zhang, Y., Bai, E., Libra, R., Rowden, R., and Liu, H., 1996. Simulation of spring discharge from a limestone aquifer in Iowa, USA. *Hydrogeology Journal*, 4(4), 41-54.

Zhang, Z., De Wulf, R. R., Van Coillie, F.M., Verbeke, L.P., De Clercq, E.M., and Ou X., 2011. Influence of different topographic correction strategies on mountain vegetation classification accuracy in the Lancang Watershed, China, *Journal of Applied Remote Sensing*, 5(1), 053512-053521

Zhao, S., 1986, *Physical Geography of China*. New York and London: Wiley, 209pp

Zhou, Y., Chen, J., Guo, Q., Cao, R., and Zhu, X., 2014. Restoration of Information Obscured by Mountainous Shadows Through Landsat TM/ETM+ Images Without the Use of DEM Data: A New Method. *IEEE Transactions on Geoscience and Remote Sensing*, 52(1): 313-328

Zheng, C., and Wang, P. P., 1999. MT3DMS: A modular three-dimensional multispecies transport model for simulation of advection, dispersion, and chemical reactions of contaminants in groundwater systems; documentation and user's guide. Alabama

University. *Technical report*, U.S. Army Engineer Research and Development Center Contract Report SERDP-99-1, Vicksburg, MS.

Zhu, X., 1982. Karst geomorphology and caves in Guilin, *Annals of the Academy of Geologic Science of China*. Geologic Printing House, Beijing, 149-150

Zhu, X., 1988. *Guilin karst*. Shanghai: Scientific & Technical Publishers, 188pp.

Zhu, X., Wang, X., Zhu, D., and Qin, H., 1988. *Study on Karst geomorphology and caves in Guilin*, Geological Publishing House, Beijing, 249 pp

Zhu, X., Zhu, D., and Ru, J., 1980. *Geomorphology of tower karst and its development in Guilin: Collected Papers of the International Geological Journal (5)*. Geologic Printing House, Beijing, 98-108.

Zhu, X., Zhu, D., Zhang, Y., Lynch E.M., 2013. Tower karst and cone karst. In: *Treatise on Geomorphology*, ed. Shroder, J.F. Academic Press, San Diego, pp. 327–340.

CURRICULUM VITAE

Wei Huang

Place of birth: Guiyang, the People's Republic of China

Education

B.E., Hefei University of Technology, China, July 2002
Major: Biology Engineering and Food Science

M.S., Ibaraki University, Mar 2009
Major: Bio-Resource Science

Ph.D., University of Wisconsin-Milwaukee, Dec 2014
Major: Geography

Dissertation Title:

Spatial Dimensions of Tower and Cockpit Karst: A Case Study
of Guilin, China